NACA RM L57F06

NACA

RESEARCH MEMORANDUM

AERODYNAMIC HEATING OF A THIN, UNSWEPT, UNTAPERED, MULTIWEB, ALUMINUM-ALLOY WING AT MACH NUMBERS UP TO 2.67 AS DETERMINED FROM A FREE-FLIGHT INVESTIGATION OF A ROCKET-PROPELLED MODEL

By H. Kurt Strass and Emily W. Stephens

Langley Aeronautical Laboratory
Langley Field, Va.

NATIONAL ADVISORY COMMITTEE FOR AERONAUTICS

WASHINGTON

August 6, 1957
Declassified January 7, 1959

NACA RM L57F06

NATIONAL ADVISORY COMMITTEE FOR AERONAUTICS

RESEARCH MEMORANDUM

AERODYNAMIC HEATING OF A THIN, UNSWEPT, UNTAPERED, MULTIWEB, ALUMINUM-ALLOY WING AT MACH NUMBERS UP TO 2.67 AS DETERMINED FROM A FREE-FLIGHT INVESTIGATION OF A ROCKET-PROPELLED MODEL

By H. Kurt Strass and Emily W. Stephens

SUMMARY

A free-flight investigation has been made on a multiweb aluminum-alloy wing at essentially zero-lift conditions to determine the aerodynamic heat-transfer characteristics and transient temperature distribution. The test wing was unswept and untapered, having a 20-inch chord, a 20-inch exposed semispan, and a circular-arc airfoil section with a thickness of 5 percent. The tests were conducted on a rocket-propelled model up to a Mach number of 2.67 and a Reynolds number of 16.0×10^6 based on a length of 1 foot. The test wing was also instrumented to detect flutter, but none was observed at any time during the flight test.

Comparisons made between experimental values of Stanton number and values obtained by the use of the theory of Van Driest for laminar and turbulent boundary layers show reasonably good agreement between the measured values and the theoretical turbulent values. Temperature measurements made at the web center line on one of the spanwise spars agreed well with calculated values.

Stanton numbers obtained in free flight agreed well with values obtained from ground tests of an identical wing at a Mach number of 2 in the preflight jet of the Langley Pilotless Aircraft Research Station at Wallops Island, Va.

INTRODUCTION

As part of a general program by the Langley Pilotless Aircraft Research Division to determine heat-transfer and structural characteristics of aircraft components at supersonic speeds, temperature and vibration measurements were made on a multiweb aluminum-alloy wing mounted as one of the stabilizing wings of a rocket-propelled test vehicle. The test wing was unswept and untapered, having a 20-inch chord, a 20-inch exposed semispan, and a circular-arc airfoil section with a thickness of 5 percent. A two-stage rocket-propulsion system propelled the test vehicle up to a Mach number of 2.67 and a corresponding Reynolds number of 16.0×10^6 based on a length of 1 foot.

The heat-transfer data calculated from measured temperatures are compared with values calculated by the theory of Van Driest for a flat plate with laminar and turbulent boundary layers. In addition, the heat-transfer data from the flight test are compared with data obtained from the Langley Structures Research Division of ground tests of an identical wing at a Mach number approximately equal to 1.99 in the preflight jet of the Langley Pilotless Aircraft Research Station at Wallops Island, Va. The stream static pressure is maintained at about 1 atmosphere, the free-stream temperature at about 75° F, and the stagnation temperature at approximately 500° F (ref. 1). Both tests were conducted at the Langley Pilotless Aircraft Research Station at Wallops Island, Va.

SYMBOLS

C_f	local skin-friction coefficient
c_p	specific heat of air at constant pressure, Btu/(slug)(°F)
h	local heat-transfer coefficient, Btu/(sec)(sq ft)(°F)
h_j	interface conductance, Btu/(sq ft)(hr)(°F)
M	Mach number
N_{St}	Stanton number, $\frac{h}{c_p \rho V}$
q	dynamic pressure, lb/sq ft
R	Reynolds number, $\frac{\rho V}{\mu} \frac{x}{12}$

t	time, sec
T	temperature, °F
V	velocity, ft/sec
x	distance from wing leading edge (measured in free-stream direction), in.
y	distance from wing tip (measured normal to model center line), in.
ρ	density, slugs/cu ft
μ	viscosity, slugs/ft-sec

Subscripts:

l	local
s	skin
stag	stagnation
∞	free-stream conditions

TEST VEHICLE AND TECHNIQUE

Model

The test vehicle used in this investigation is described in figures 1 to 4 by means of photographs and dimensional sketches. The test wing was one of four stabilizing wings mounted on a rocket-propelled test vehicle. The wings were identical in all respects except that the noninstrumented wings were constructed to have greater stiffness than the test wing by means of two additional chordwise ribs per wing in order to minimize the chances of loss of data resulting from premature failure of the noninstrumented wings. The wings were unswept and untapered, having a 20-inch chord, a 20-inch exposed semispan (fig. 3), and a circular-arc airfoil section with a thickness of 5 percent. The wings were made of 2024-T3 aluminum alloy and had 0.064-inch-thick skins, six 0.025-inch-thick internal spars, and solid leading- and trailing-edge pieces. All rivet heads were ground flush with the wing surface and the entire surface of the test wing was given a finish equivalent to a smooth grind (roughness equal to approximately 35 microinches). A more complete description of the test wing is given in figure 4.

The wing was a duplicate of one previously tested by the Langley Structures Research Division at $M \approx 1.99$. in the preflight jet of the Langley Pilotless Aircraft Research Station at Wallops Island, Va. A good description of the test facility and the general procedure may be obtained from previous tests of a similar nature which are described in reference 1.

The wings were mounted on the test vehicle in a manner very similar to that employed in the ground test. Although no structural tests were made of the flight-tested wing, the rigidity of the root mounting is not believed to be significantly different from the ground-tested wing.

Test-Vehicle Instrumentation

Wing temperatures were measured with 24 iron-constantan thermocouples arranged as shown in figure 5. Twenty-one were located in the skin approximately midway between the spanwise spars and three on a spar web between stations 5 and 6 at the wing-chord plane. The thermocouples were installed by drilling a tapered hole through the skin with the larger diameter on the outer surface of the skin. The thermocouple wires were passed through the hole, knotted together, and drawn back into the metal. The metal was then puddled into intimate contact with the thermocouple by making use of a helium-shielded arc-welding process. Calculations indicate that the thermocouple temperatures were negligibly affected by conduction effects. The outputs from these thermocouples in conjunction with three reference voltages were commutated and transmitted over two telemeter channels. The commutation rate was such that the temperature at any given station, including the reference voltages, could be read approximately five times a second. The reference voltages were obtained by the use of a mercury cell and a voltage dividing network designed to supply a range of voltages equivalent to the temperature range that the thermocouples were expected to cover. These reference voltages provided a method for checking the calibration of the thermocouples in flight.

Although no flutter was evident in the previously mentioned preflight-jet tests of a wing identical to that used in the rocket-model tests, there was no assurance that flutter would not occur at the higher speeds of the flight test. Consequently, the wing was instrumented with two flutter detecting gages attached to the skin at the positions also shown in figure 5. These gages were essentially uncalibrated strain gages used only for detecting the frequency of strain reversals which would be evident in case the wing was subject to a violent fluttering motion. The locations of the gages were selected on the basis of preflight-jet tests of a slightly different wing which fluttered and showed that a region of great stress was located near the wing tip caused by a violent chordwise deformation during flutter. (See ref. 2.)

Measurements of longitudinal acceleration and dynamic pressure were also telemetered during flight.

Flight-Test Technique

The model was launched at an elevation angle of 25°. A two-stage rocket-propulsion system was used. (See fig. 6.) The first stage was made up of two ABL Deacon rocket motors strapped together and fired simultaneously. This stage propelled the model to a Mach number of approximately 1.6, whereupon a drag separation occurred at first-stage burnout. The test vehicle was then propelled to a Mach number of approximately 2.7 by the JATO, 6-KS-3000, T-40 second-stage rocket motor. Data were obtained until the model had decelerated to $M \approx 1.2$.

True air velocity data were obtained by correcting the velocity measured by CW Doppler velocimeter for angular deviation of the flight path relative to the radar transmitter and for winds at altitude by the use of space coordinates measured by an NACA modified SCR-584 tracking radar and atmospheric and wind conditions obtained by radiosondes launched immediately after the test flight and tracked by a Rawin set AN/GMD-1A.

Figure 7 presents time histories of the most important flight-test parameters. The telemetered values of longitudinal acceleration and dynamic pressure were not used in this paper because the values of velocity obtained from these measurements were less accurate than those obtained from the ground-based measurements. These instruments were included in the test vehicle for use in case no velocity data were obtained from the CW Doppler velocimeter. The maximum altitude attained by the test vehicle was approximately 5,000 feet. All data were obtained at essentially zero-lift conditions.

PRECISION

The probable maximum errors which exist in these data are estimated to be as follows:

ΔT_s, °F	±5
ΔT_∞, °F	±5
ΔV_∞, ft/sec	±4.0
$\Delta\rho$, slug/cu ft	±0.0003
ΔM	±0.01
ΔN_{St}	±0.00009 (valid for time intervals between 6 and 11 seconds and greater than 16 seconds)

RESULTS AND DISCUSSION

No evidence of wing flutter was observed at any time during the flight test. The measured temperature-time histories are shown in figure 8. The web temperatures were measured at the center of the web of the spanwise spar located approximately midway between stations 5 and 6. In order to illustrate the relationship between the temperatures in the web and in the adjacent skin, the web temperatures at row 2 are typical and are compared in figure 9 with the adjacent skin temperatures at row 2. The web temperatures are 60° to 150° lower than the mean point between stations 5 and 6 at any instant up to and including the time where maximum skin temperature was recorded (approximately 13.5 seconds). The maximum web temperatures were approximately 60° lower than the maximum skin temperatures which averaged about 465° F for the three rows.

Heat Transfer

Figure 10 presents the measured variation of Stanton number with time as compared with the theory of Van Driest for laminar and turbulent boundary layers for the three spanwise locations. The laminar values were computed by using the method of reference 3. The turbulent values were computed by using the method of reference 4 in which the Von Kármán similarity law for mixing length and a Reynolds analogy factor based upon laminar and turbulent Prandtl numbers equal to 0.71 and 0.86, respectively, are assumed. The theoretical ratio of Stanton number to skin-friction coefficient based on these assumptions varied from 0.602 to 0.605 for the local experimental Reynolds number range for which temperature data are presented. For purposes of calculation, a constant value of 0.60 was used which agrees well with the average experimentally determined ratio of 0.61 given in reference 5. The recovery factor was assumed to be constant for the purposes of data reduction and equal to 0.89 or $(\text{Prandtl no.})^{1/3}$, the theoretical recovery factor for a turbulent boundary layer. This recovery factor is in fair agreement with an average value of 0.85 ±0.03 as determined from this test, neglecting radiation and conduction effects which were determined to be negligible.

The method whereby the skin temperature-time data were reduced to Stanton number is well described in the literature of which reference 6 is a good example. Both the theoretical and experimental values of Stanton number were based on the local aerodynamic conditions calculated from two-dimensional shock-expansion theory. Locations near the wing tip were corrected for three-dimensional effects by the method of reference 7. The overall effect of these corrections upon Stanton number was negligible for the conditions of this test. The material properties of 2024-T3 aluminum alloy were obtained from reference 8. No corrections for conductivity within the skin or radiation of heat from the skin were made as

calculations indicated that the effect of conductivity was well within the accuracy of the test and the effect of radiation was negligible at these heating rates and skin temperatures.

The values of the experimentally determined Stanton numbers became increasingly unreliable as the skin temperatures approached the temperature of air in the boundary layer. For this reason, values of Stanton numbers (fig. 10) in the vicinity of 13.5 seconds deviated widely from the trend of the data immediately preceding and following this time. In general, the measured values are in reasonably good agreement with the theoretical turbulent boundary-layer values. With the exception of a few random points which are less than turbulent theory but much greater than laminar theory, the data indicate that the boundary layer must be turbulent nearly everywhere on the test wing. Spanwise effects upon measured Stanton number were small. A decrease of approximately 10 percent is evident for the locations nearest the wing-fuselage juncture (row 3). Detailed calculations show that the heat conduction into the wing-root juncture was negligible. This calculation procedure was similar to that described elsewhere in this paper with regard to temperature estimation at web center line.

Stations near the leading edge were generally in better agreement with turbulent theory than those near the trailing edge (fig. 10). Experimental data in reference 5 suggest that an appreciable decrease in the ratio of Stanton number to skin-friction coefficient occurs with increasing Reynolds number. The importance of the data of reference 5 if verified by subsequent experiment is highlighted by a reduction of greater than 20 percent in this ratio as Reynolds number was increased from 2×10^6 to 24×10^6. This reduction would be evidenced as a corresponding decrease in heat transfer.

Although the accuracy of the present analysis does not warrant drawing definite conclusions regarding the effect of Reynolds number upon the ratio of Stanton number to skin-friction coefficient, a tentative correlation does show a tendency for this ratio to decrease with increasing local Reynolds number for local Reynolds numbers up to approximately 20×10^6.

The experimental data and turbulent theoretical values of Stanton number from figure 10 which were based on $\frac{N_{St}}{C_f} = 0.60$ are presented in figure 11 as a function of the distance from wing leading edge for the three spanwise locations for several typical times during the flight test. For comparison, turbulent theoretical values are also shown which were based on

$$\frac{N_{St}}{C_f} = f(R_l)$$

and the data of reference 5. In general, the chordwise trend is better described by the calculations based on $\frac{N_{St}}{C_f} = f(R_l)$.

Skin and Web Temperatures

A comparison of the measured chordwise temperature distribution with calculated values is shown in figure 12 for the three spanwise locations and for several typical times during the flight test. The temperature calculations were made by employing iteration methods and by neglecting temperature gradients within the skin and, for the purpose of this figure, the temperature variations near the spars, which are discussed in a subsequent section in this paper, have been ignored. The calculated values overestimate the temperature change slightly, an effect which is cumulative and leads to an appreciable discrepancy in absolute magnitude between calculated and measured values after an extended period of time. For example, the calculated temperatures assuming $\frac{N_{St}}{C_f} = 0.60$ at 11 seconds averaged 25° F higher than the measured values but the chordwise variation was in good agreement (fig. 12(d)). At a later time (18 seconds, fig. 12(f)) when the test wing was undergoing a cooling phase, the measured and calculated chordwise temperature variations were in relatively poor agreement. The apparent good agreement at station 1 is fortuitous and results primarily from an appreciable overestimation of the heat transfer at this point near this time. (See fig. 10(a).)

An improvement was evident (fig. 12) in the trend of the calculated chordwise temperatures when the calculations were made by assuming $\frac{N_{St}}{C_f} = f(R_l)$. Near the trailing edge the discrepancy between measured and calculated temperatures was nearly halved compared with calculations assuming $\frac{N_{St}}{C_f} = 0.60$.

Figure 13 presents a comparison of the experimental data of figure 9 with calculated values for the same thermocouple locations. For purposes of calculation, the cross section of the structure was divided into 17 elements as shown in figure 14 and the temperatures in each element computed by a method similar to that described in reference 9. The calculations were performed on the IBM 650 Digital Computer. The experimental values of the heat-transfer coefficient measured in this test were

used at stations 5 and 6 (elements 1 and 12 in fig. 14). The heat-transfer coefficients applicable to elements 2 to 11 were obtained by linear interpolation. The values presented in figure 13 were calculated by assuming an interface conductance between elements 6 and 14 and elements 7 and 13 equal to 300, a more or less average value obtained from reference 11 for riveted aluminum-aluminum joints. This value of interface conductance was apparently approximately correct for this wing as the calculated temperatures for the web center line are in good agreement with measured values. In addition, in figure 13 are calculations assuming that the joint conductivity parameter $h_j = \infty$ and shows negligible change in the temperatures at thermocouple stations 5 and 6 indicating that conduction effects upon measured temperatures are negligible. Figure 15 presents the calculated skin temperatures for locations between thermocouple stations 5 and 6 and shows the effect of heat conduction into the spar for three typical times during the test. These calculations indicated that the skin temperatures nearest the spar were approximately 10° to 20° lower than the values for the insulated skin at the same location.

Comparison With Preflight-Jet Tests

The wing plan form of the ground-tested wing showing thermocouple locations is presented in figure 16. An illustrative comparison of the measured temperatures and heat-transfer coefficients obtained in flight with values obtained in preflight jet is given in figures 17 and 18 for comparable locations on the test wings. Little heating occurred during the initial portion of the flight test as the model was being accelerated up to the desired speed region whereas the ground-tested wing was subject to high heating conditions within a second of the start of the test. As a consequence the temperature-time curve from the preflight-jet test was arbitrarily shifted 2 seconds in time in order to provide a more realistic comparison with the flight-test data and shows that the temperature-time histories are roughly comparable. Figure 18 shows that in general the heat-transfer coefficients for the flight test are lower than those for the ground test as a result of the lowered air densities at the altitudes of the flight test. Measured Stanton numbers were essentially the same as evidenced by the comparison with theory of the data from both sources given in figure 19.

CONCLUSIONS

Free-flight investigation of a rocket-propelled model with an unswept, untapered, multiweb, aluminum-alloy wing employing a circular-arc airfoil section with a thickness of 5 percent has been made up to a Mach number

of 2.67 and a Reynolds number of 16.0×10^6 based on a length of 1 foot. An analysis of the data indicates the following:

(1) Experimentally determined Stanton numbers were in reasonably good agreement with the theory of Van Driest for a flat plate with turbulent boundary layer.

(2) Spanwise effects upon Stanton number were small at the conditions of this test. A decrease of approximately 10 percent was observed for the locations nearest the wing-fuselage juncture.

(3) Experimentally determined temperatures at the web center line on one of the spanwise spars agreed well with calculated values.

(4) Stanton numbers obtained in free flight agreed well with values obtained from ground tests of an identical wing in the preflight jet of the Langley Pilotless Aircraft Research Station at Wallops Island, Va., at a Mach number approximately equal to 2.

Langley Aeronautical Laboratory,
National Advisory Committee for Aeronautics,
Langley Field, Va., May 15, 1957.

REFERENCES

1. Griffith, George E., Miltonberger, Georgene H., and Rosecrans, Richard: Tests of Aerodynamically Heated Multiweb Wing Structures in a Free Jet at Mach Number 2 - Two Aluminum-Alloy Models of 20-Inch Chord With 0.064- and 0.081-Inch-Thick Skin. NACA RM L55F13, 1955.

2. Heldenfels, Richard R., and Rosecrans, Richard: Preliminary Results of Supersonic-Jet Tests of Simplified Wing Structures. NACA RM L53E26a, 1953.

3. Van Driest, E. R.: Investigation of Laminar Boundary Layer in Compressible Fluids Using the Crocco Method. NACA TN 2597, 1952.

4. Van Driest, E. R.: The Problem of Aerodynamic Heating. Aero. Eng. Rev., vol. 15, no. 10, Oct. 1956, pp. 26-41.

5. Seiff, Alvin: Examination of the Existing Data on the Heat Transfer of Turbulent Boundary Layers at Supersonic Speeds From the Point of View of Reynolds Analogy. NACA TN 3284, 1954.

6. Swanson, Andrew G., and Rumsey, Charles B.: Aerodynamic Heating of a Wing As Determined From a Free-Flight Rocket-Model Test to Mach Number 3.64. NACA RM L56F11a, 1956.

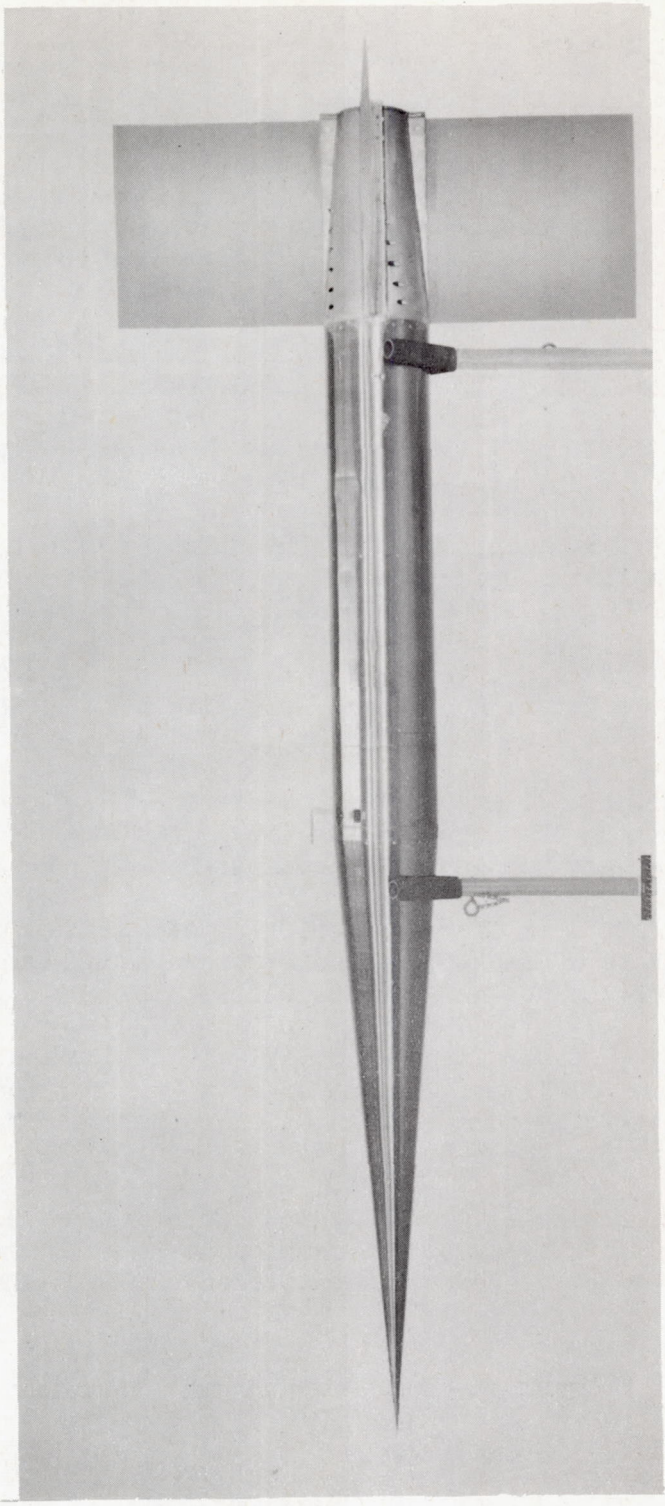
7. Czarnecki, K. R., and Mueller, James N.: An Approximate Method of Calculating Pressures in the Tip Region of a Rectangular Wing of Circular-Arc Section at Supersonic Speeds. NACA TN 2211, 1950.

8. Murmin, John J.: Thermal Properties of Aluminum and Titanium Alloys. Tech. Note WCRT 54-51, Armed Services Tech. Information Agency, Doc. Service Center (Dayton, Ohio), Mar. 1954.

9. Bartlett, G. E., Hilton, J. H., Vidal, R. J., and Woolard, H. W.: Experimental Investigations of Heat Transfer on a 10-Percent Double-Wedge Airfoil at Mach No. 2.0. Rep. No. CAL/CM-832 (Contract NOrd-14523), Cornell Aero. Lab., Inc., Jan. 1955.

10. Griffith, George E., and Miltonberger, Georgene H.: Some Effects of Joint Conductivity on the Temperatures and Thermal Stresses in Aerodynamically Heated Skin-Stiffener Combinations. NACA TN 3699, 1956.

11. Barzelay, Martin E., Tong, Kin Nee, and Holloway, George F.: Thermal Conductance of Contacts in Aircraft Joints. NACA TN 3167, 1954.



L-94361.1

Figure 1.- Test configuration.

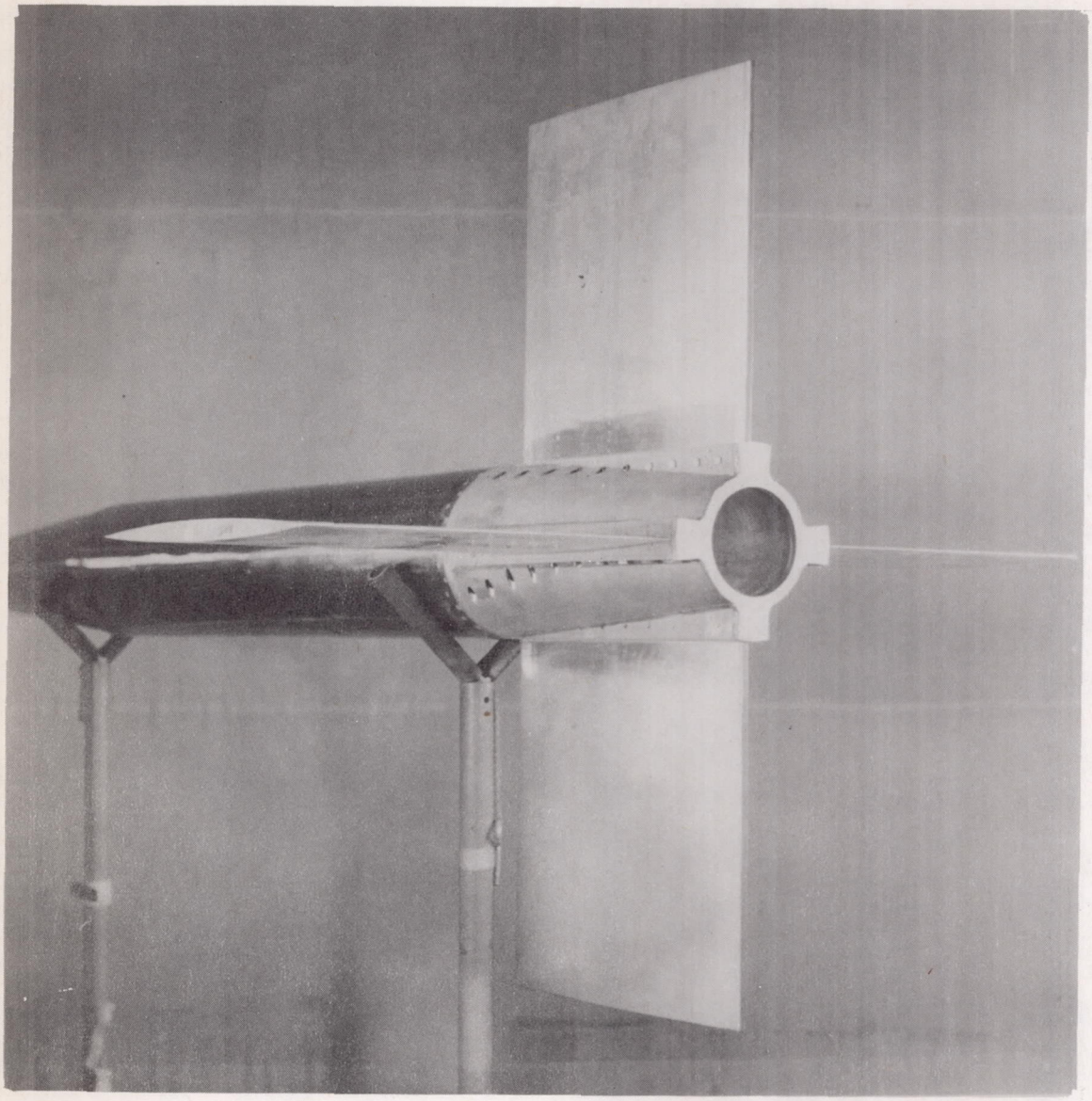


Figure 2.- Rear view of test vehicle. L-94362.1

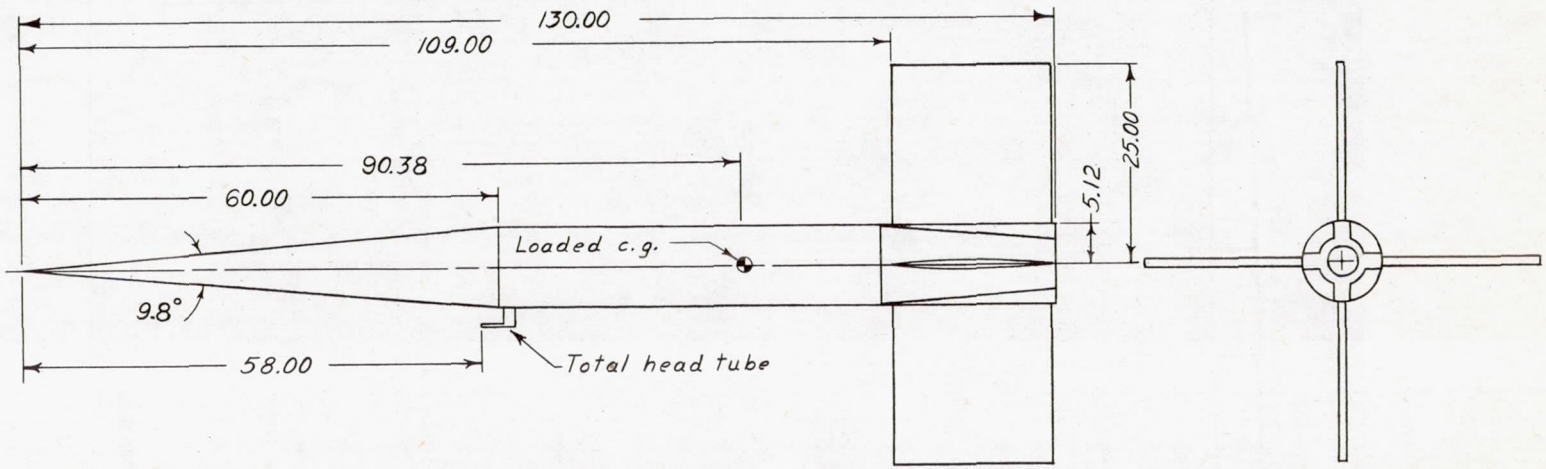


Figure 3.- General arrangement of structural test vehicle. All dimensions are in inches.

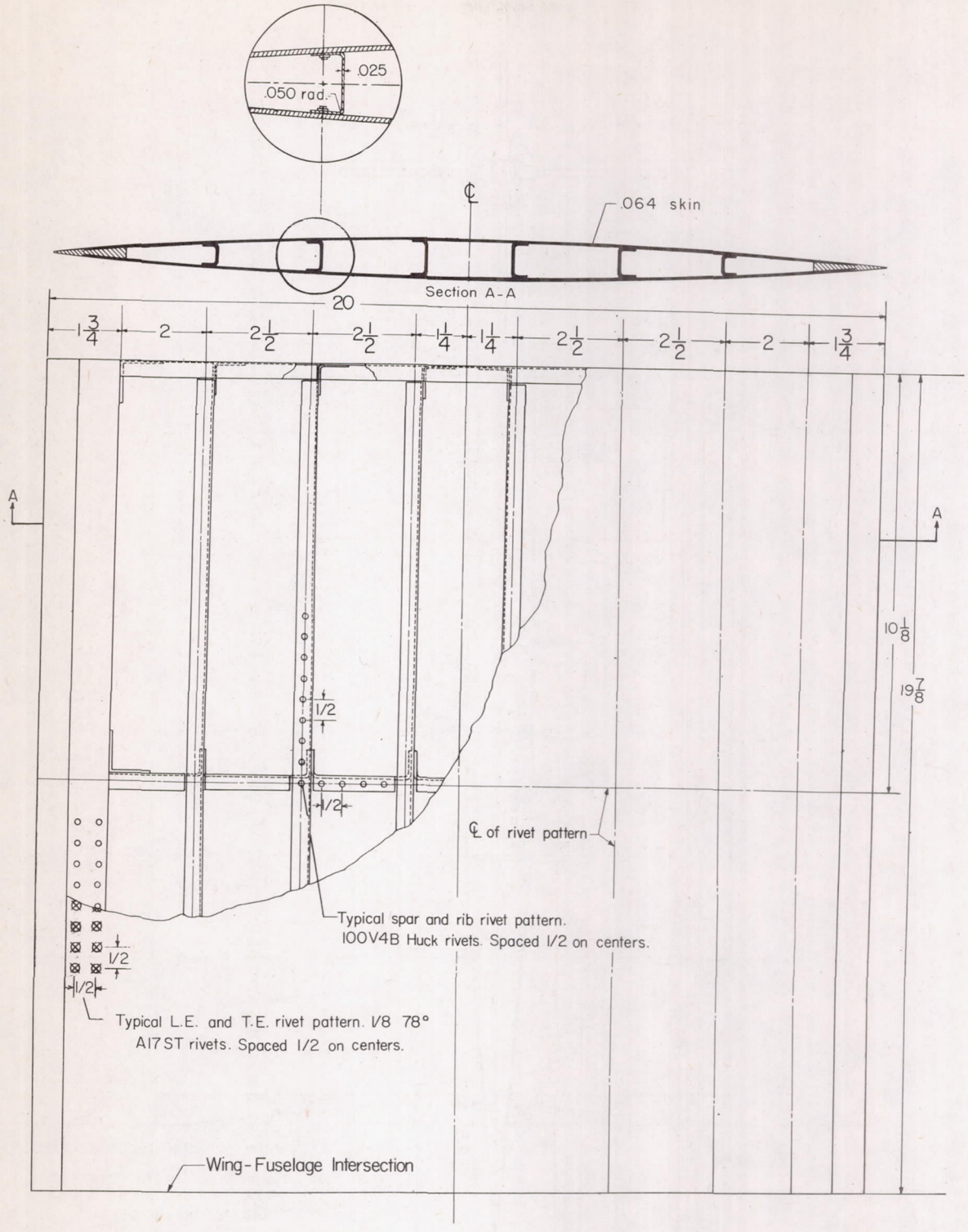


Figure 4.- Dimensions of test wing. All dimensions are in inches.

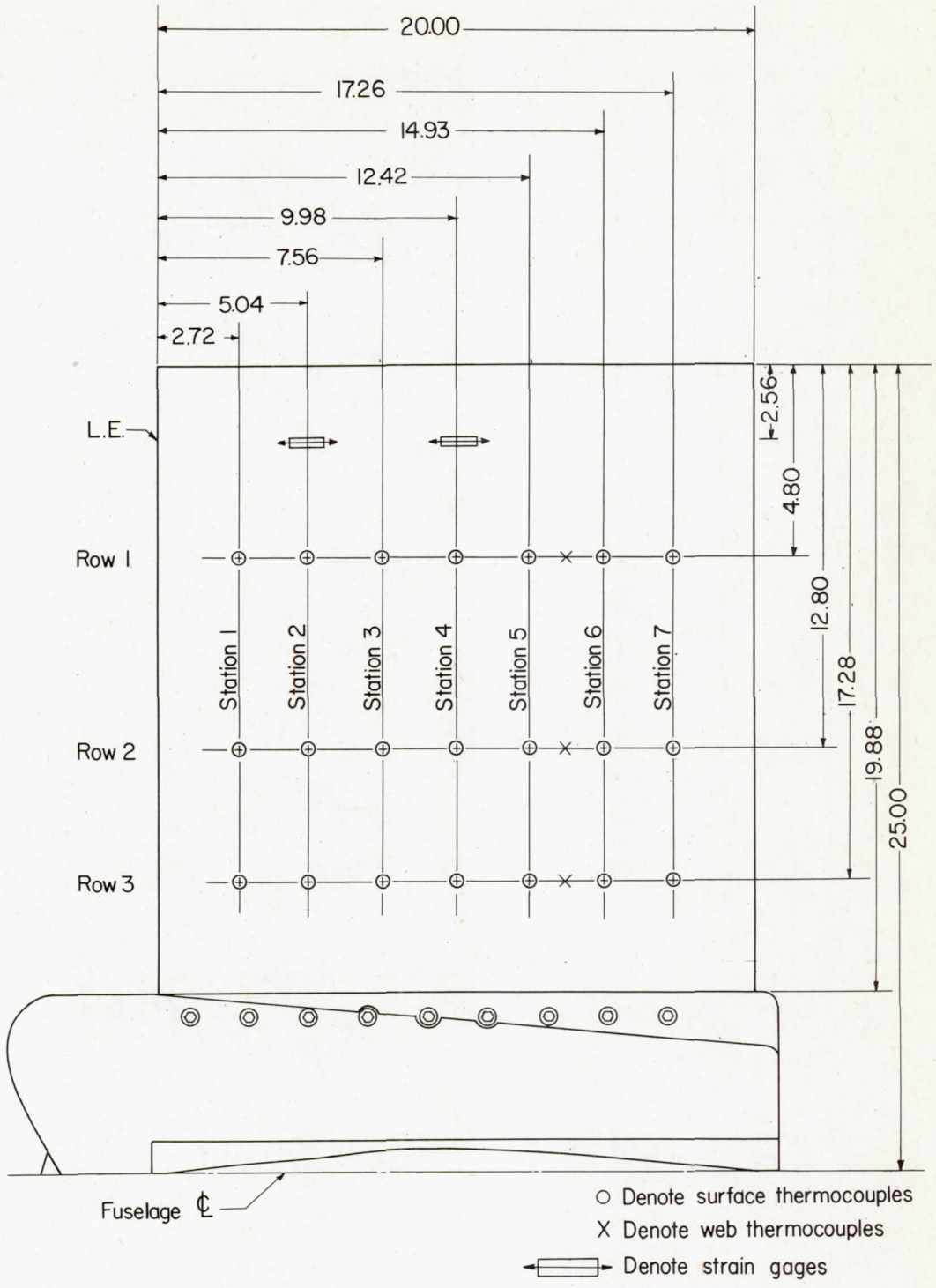
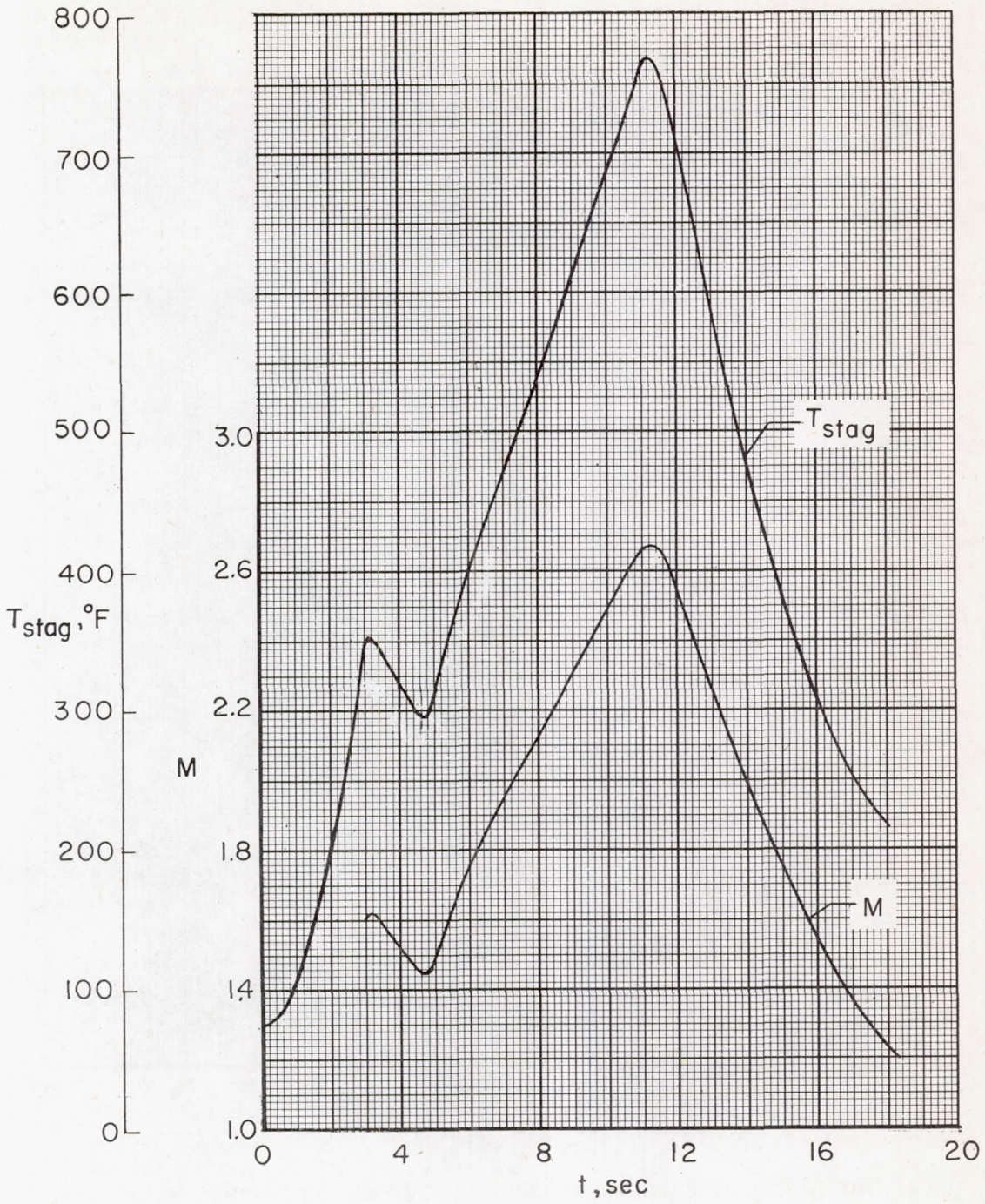


Figure 5.- Instrumentation of test wings. All dimensions are in inches.

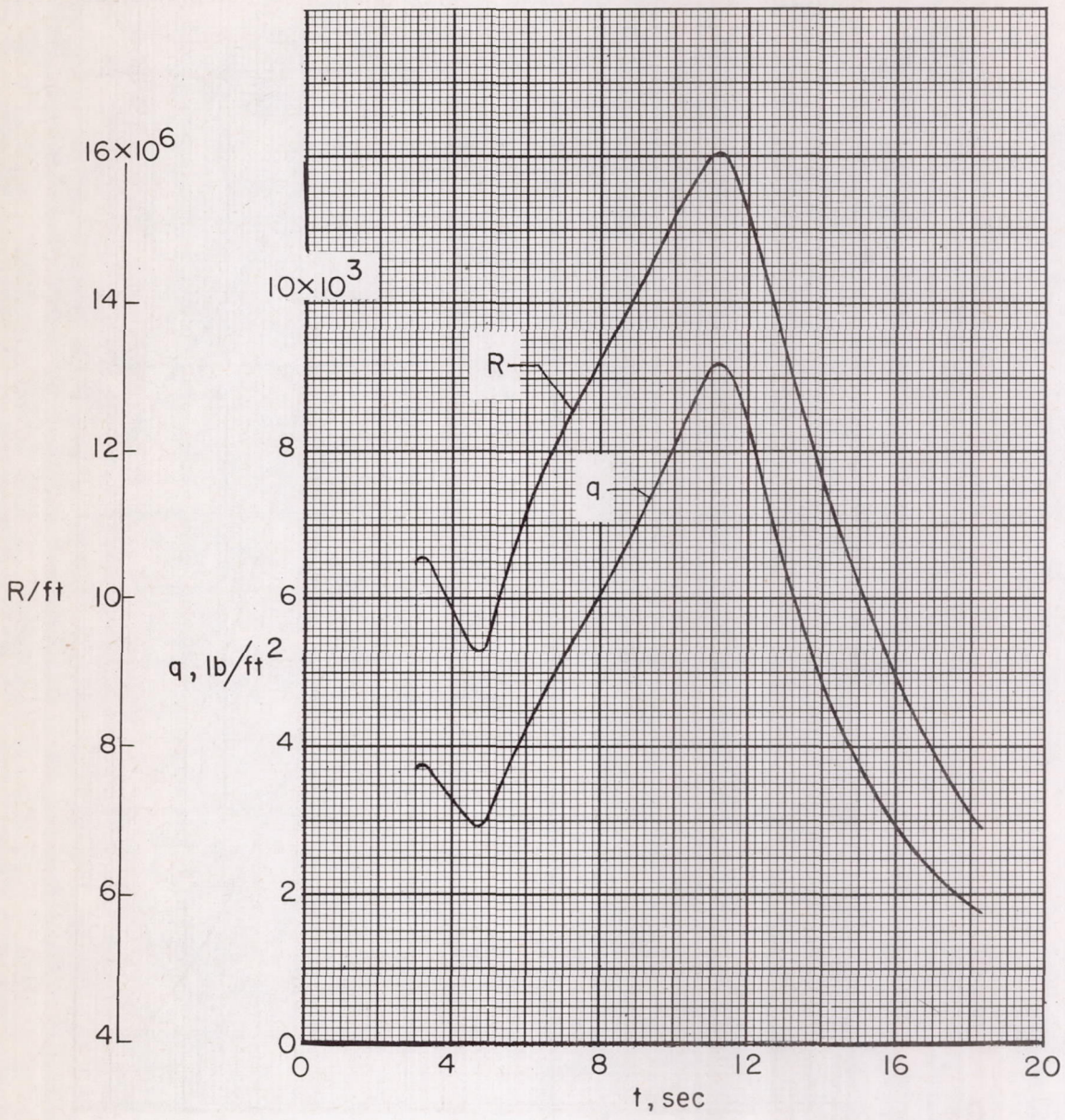


Figure 6.- Rocket model on launcher. L-94717.1



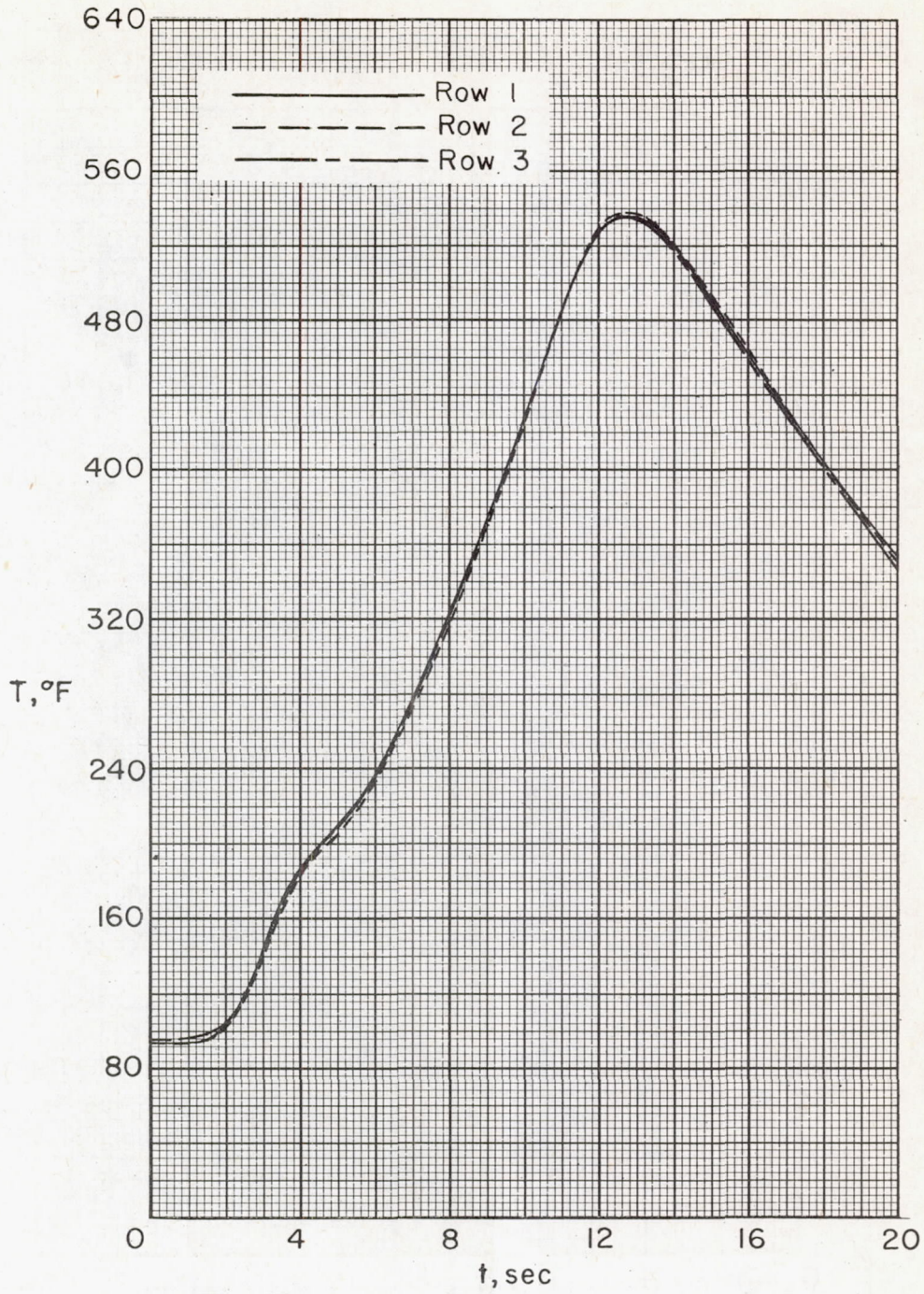
(a) Variation of stagnation temperature and Mach number with time.

Figure 7.- Time histories of several important flight parameters.



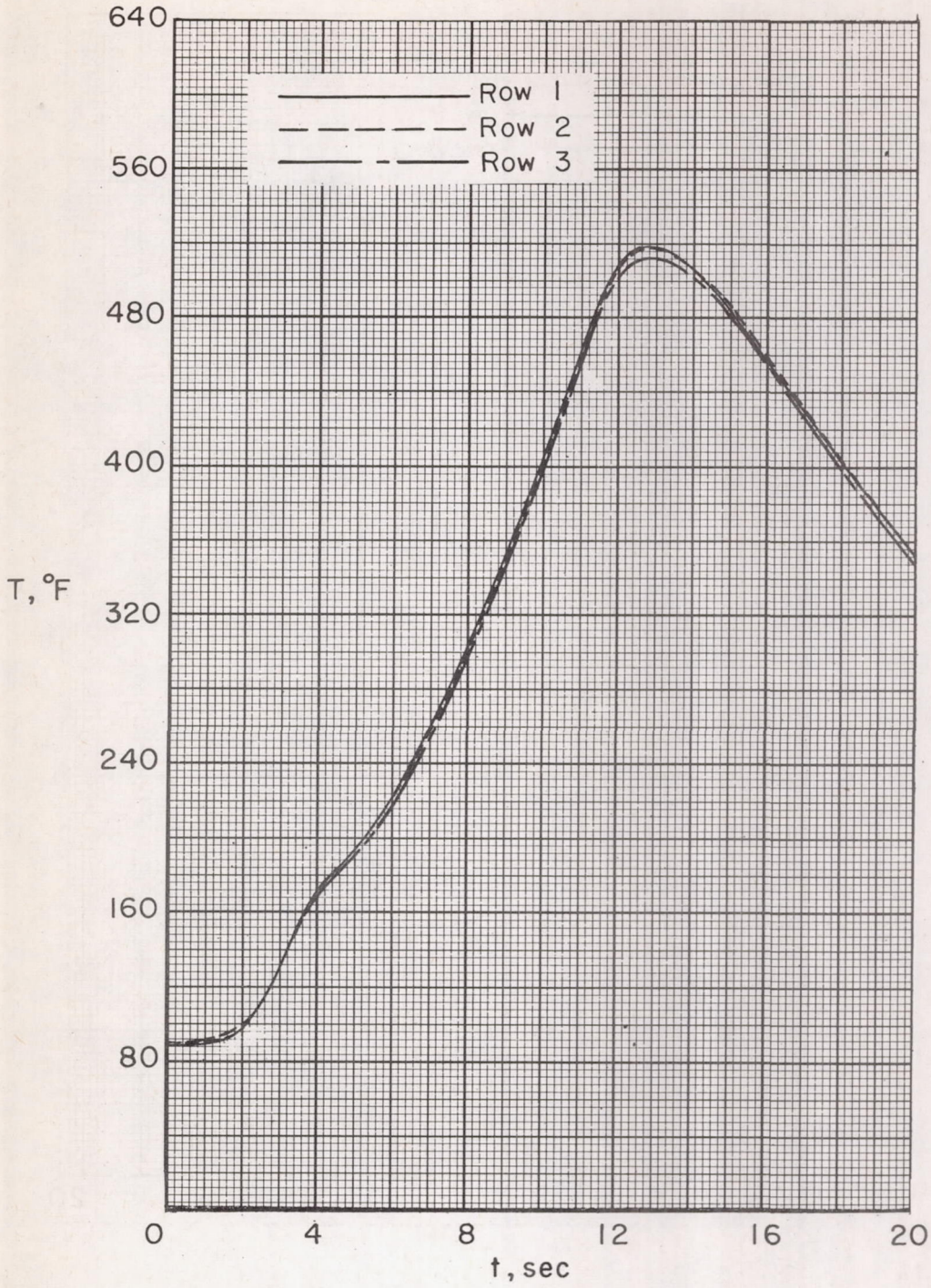
(b) Variation of Reynolds number and dynamic pressure with time.

Figure 7.- Concluded.



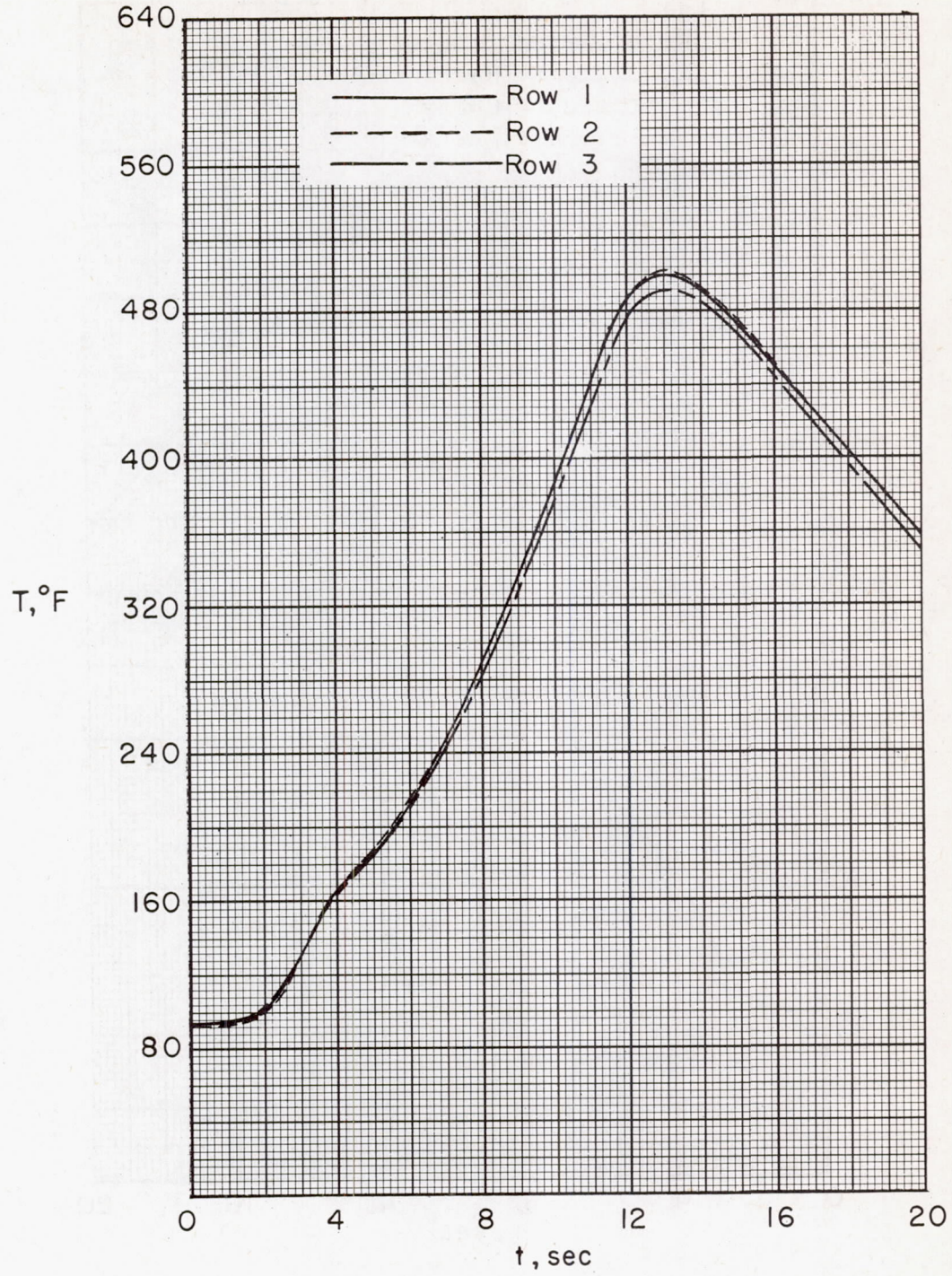
(a) Station 1; rows 1, 2, and 3.

Figure 8.- Variation of measured temperatures with time at various chordwise and spanwise stations.



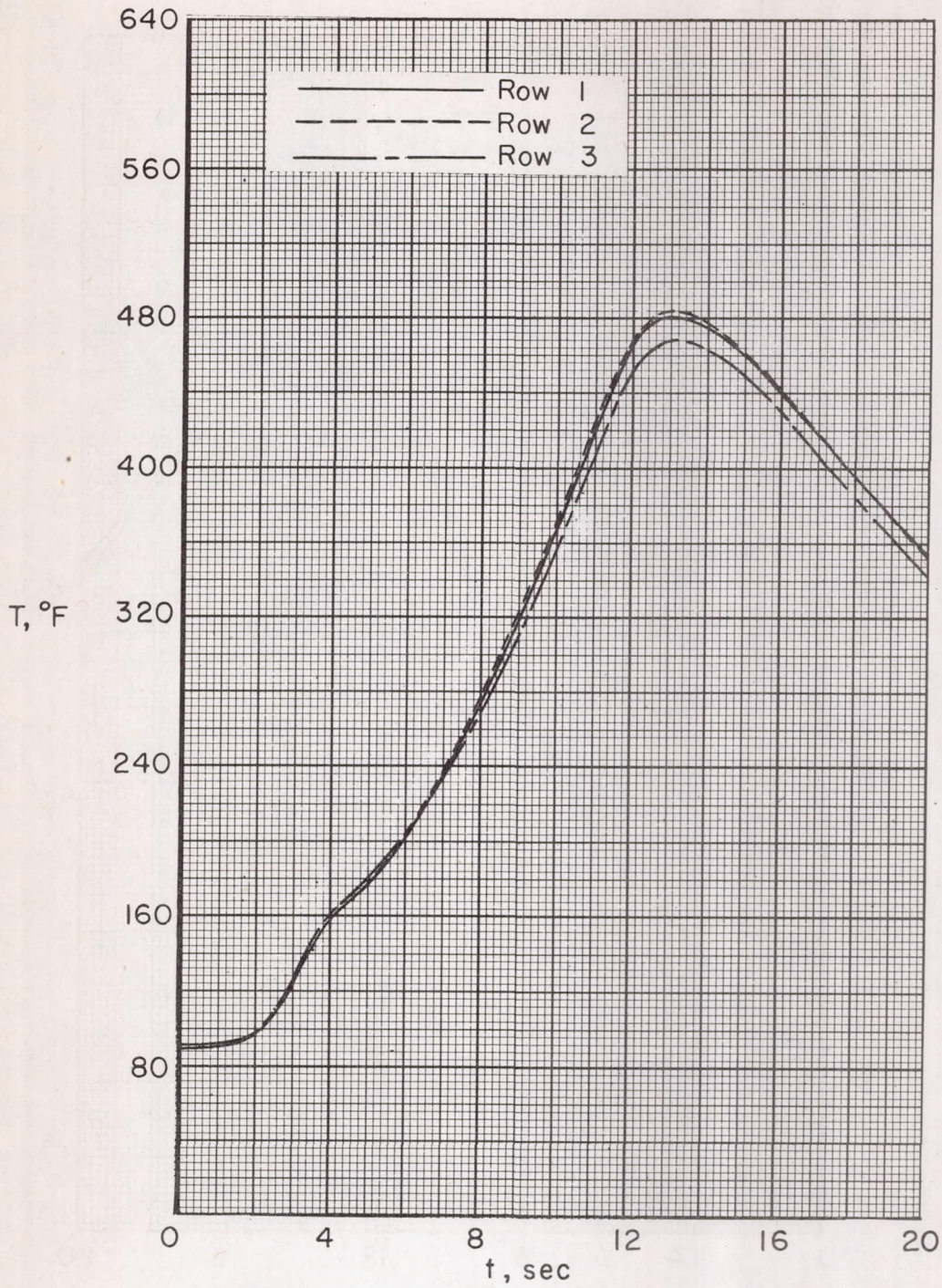
(b) Station 2; rows 1, 2, and 3.

Figure 8.- Continued.



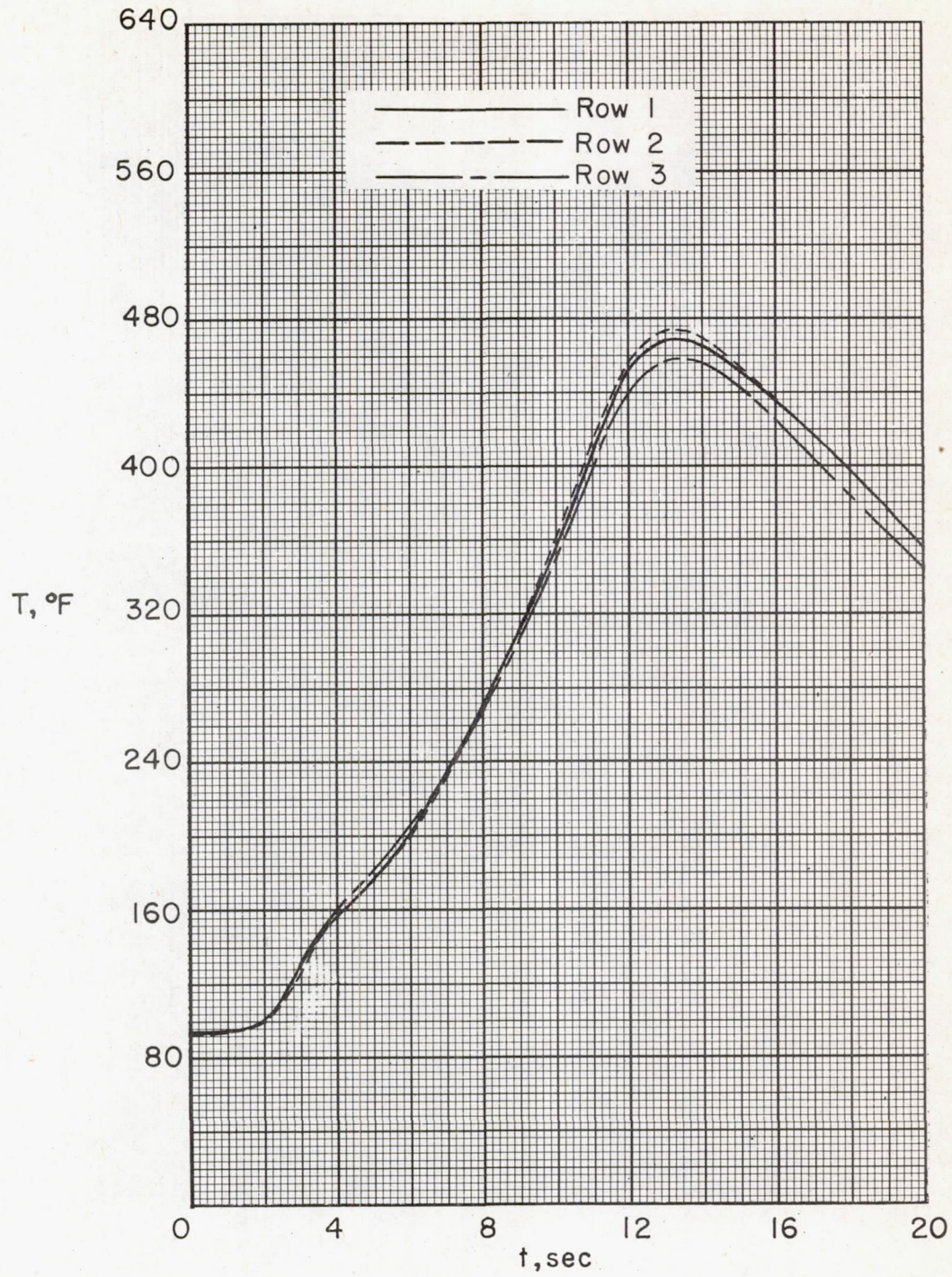
(c) Station 3; rows 1, 2, and 3.

Figure 8.- Continued.



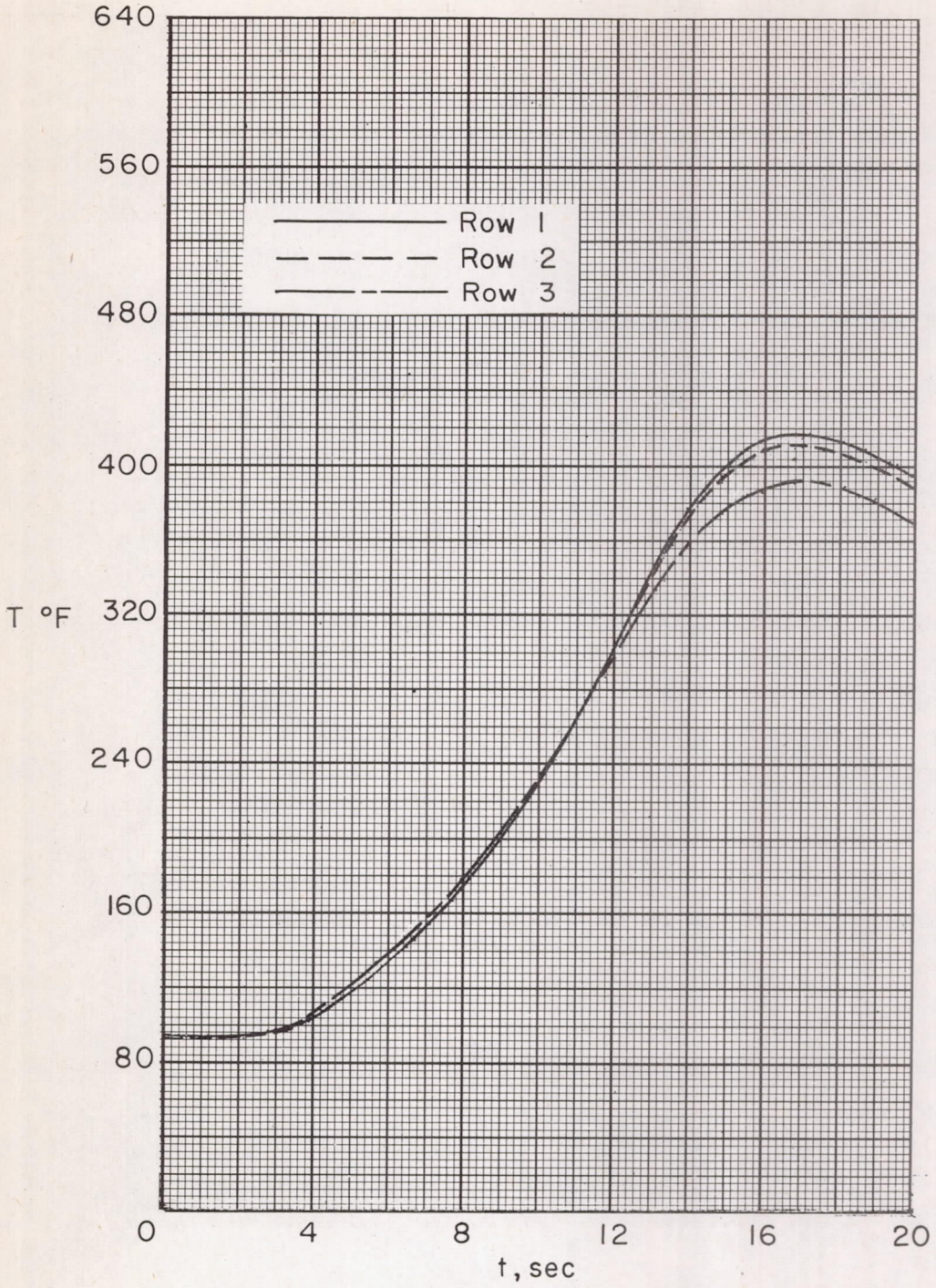
(d) Station 4; rows 1, 2, and 3.

Figure 8.- Continued.



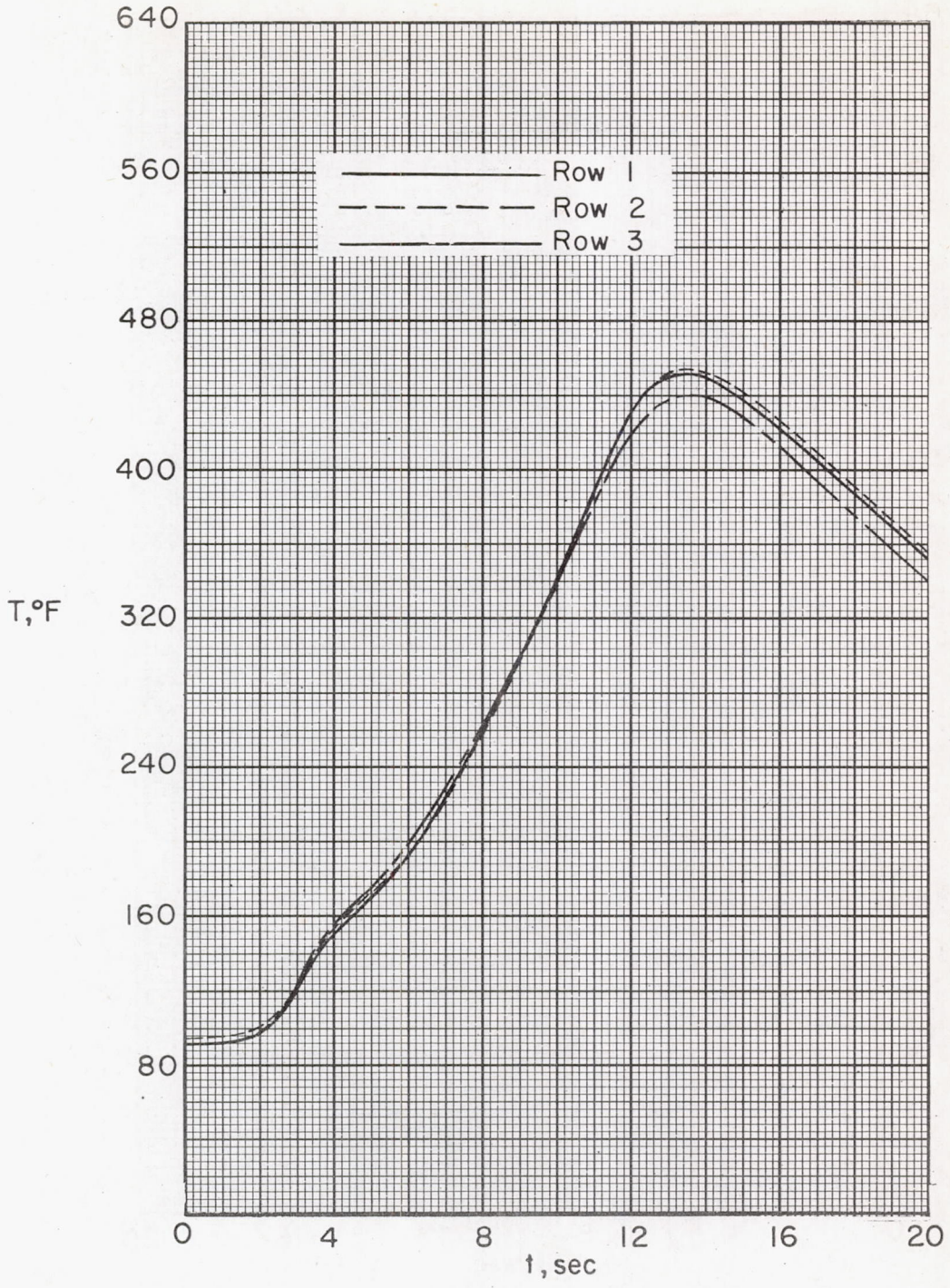
(e) Station 5; rows 1, 2, and 3.

Figure 8.- Continued.



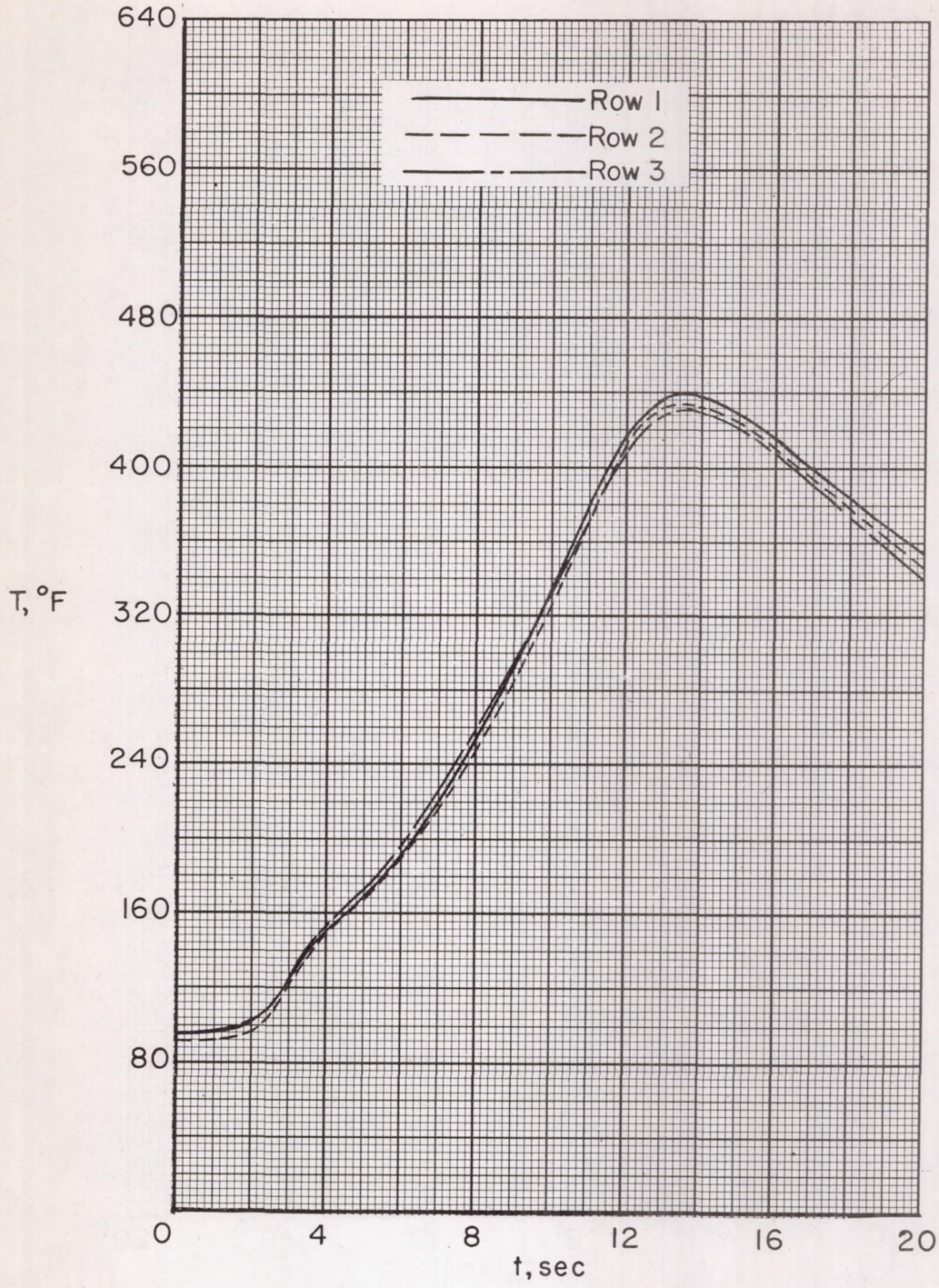
(f) Web; rows 1, 2, and 3.

Figure 8.- Continued.



(g) Station 6; rows 1, 2, and 3.

Figure 8.- Continued.



(h) Station 7; rows 1, 2, and 3.

Figure 8.- Concluded.

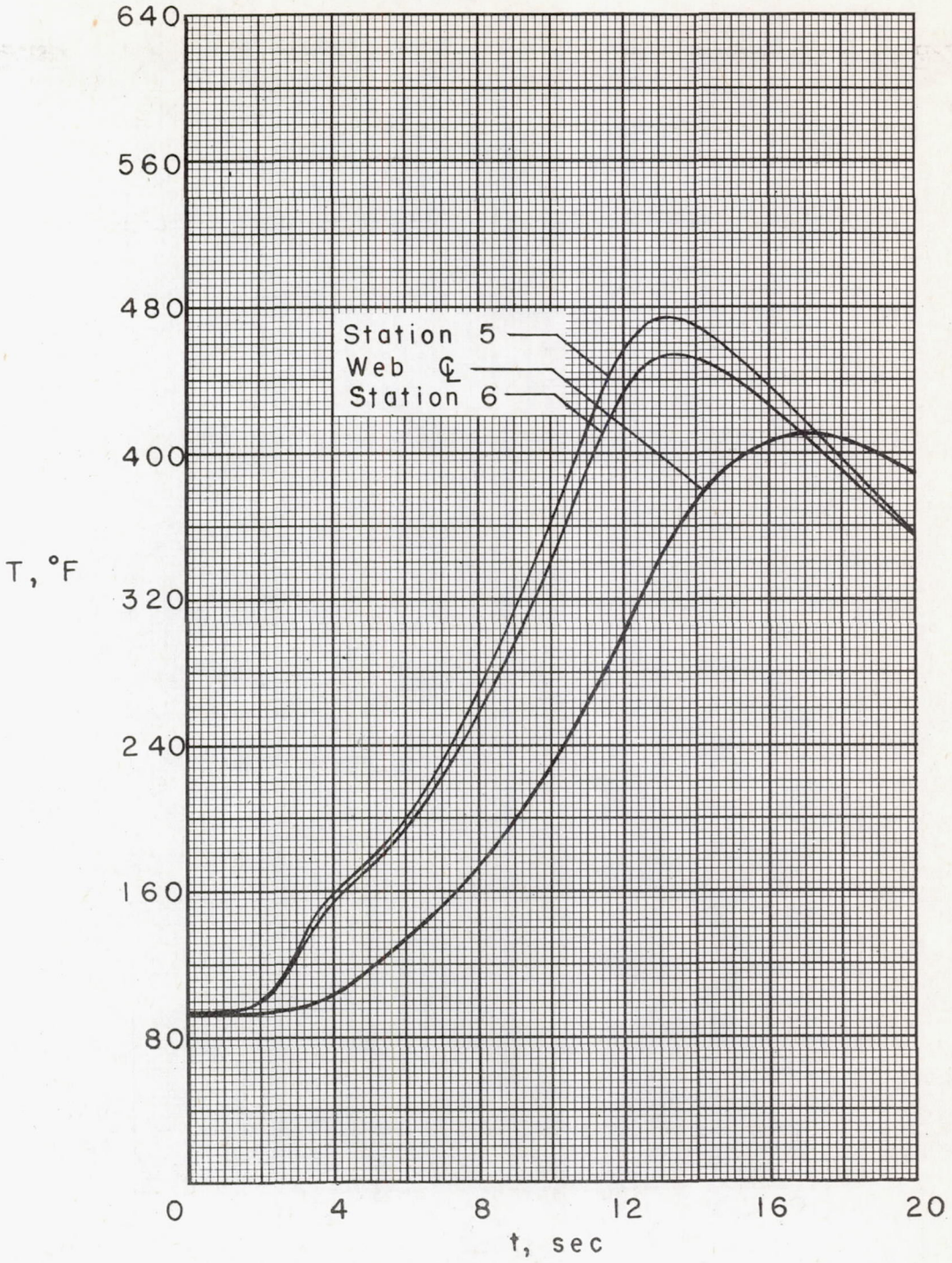
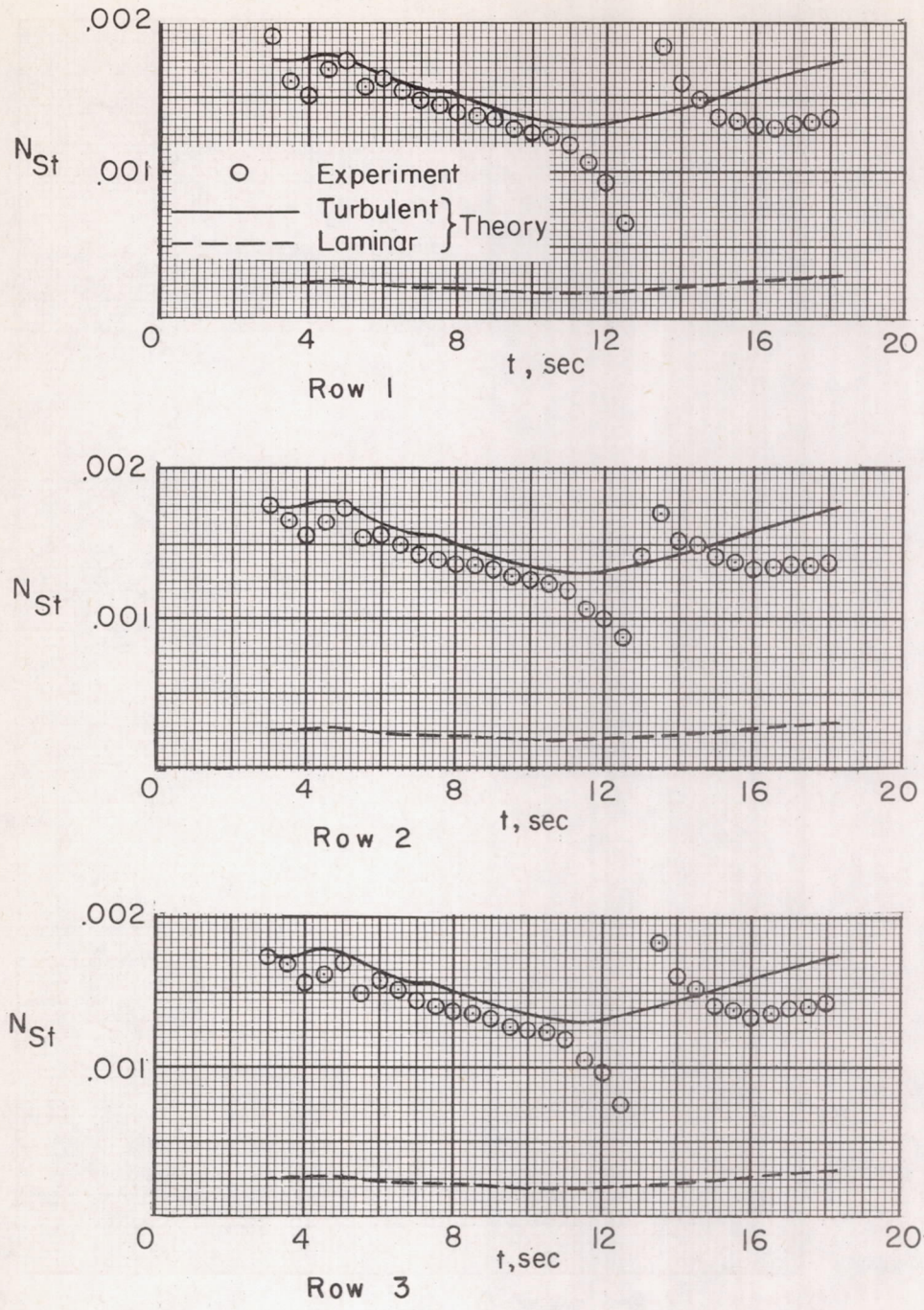
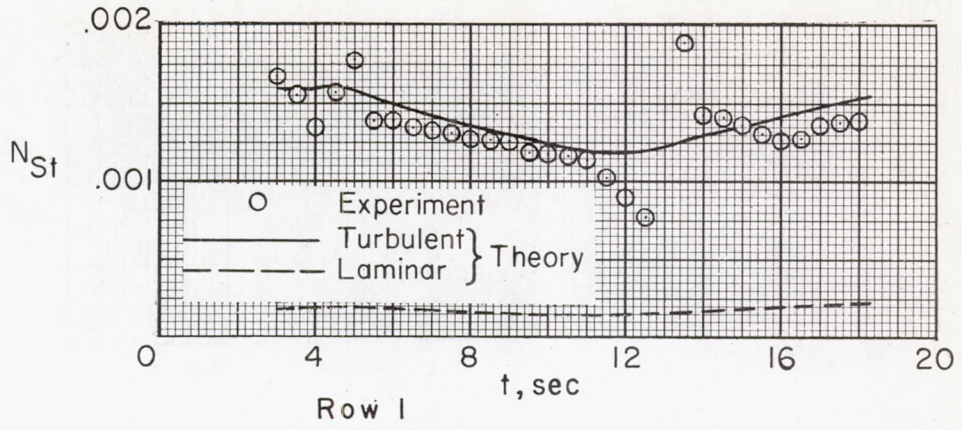


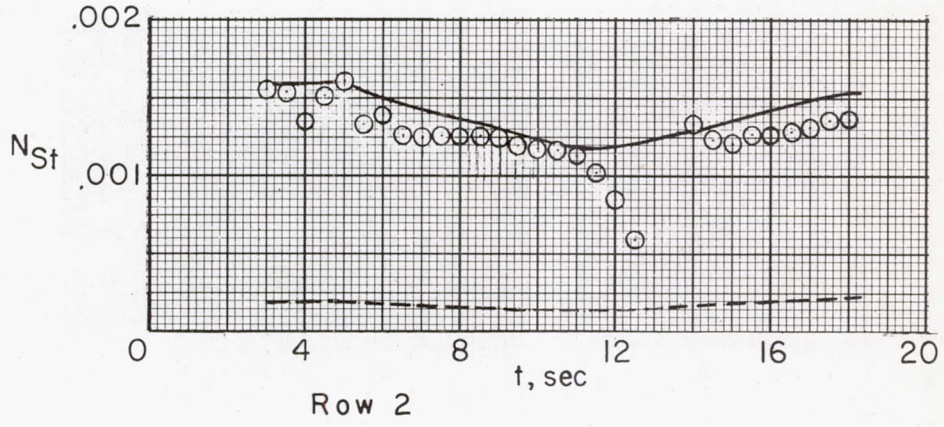
Figure 9.- Temperature values of web ℄ and row 2 of stations 5 and 6 against time.

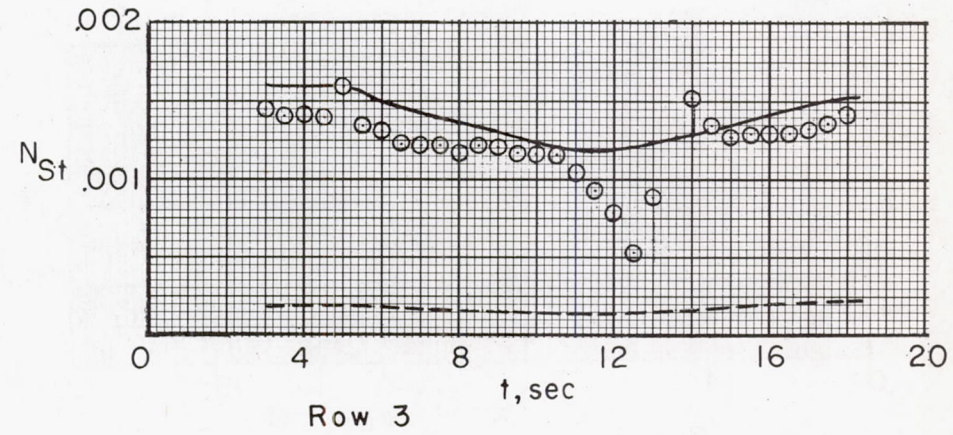


(a) Station 1.

Figure 10.- Variation of measured Stanton number with time and compared with theoretical laminar and turbulent values.

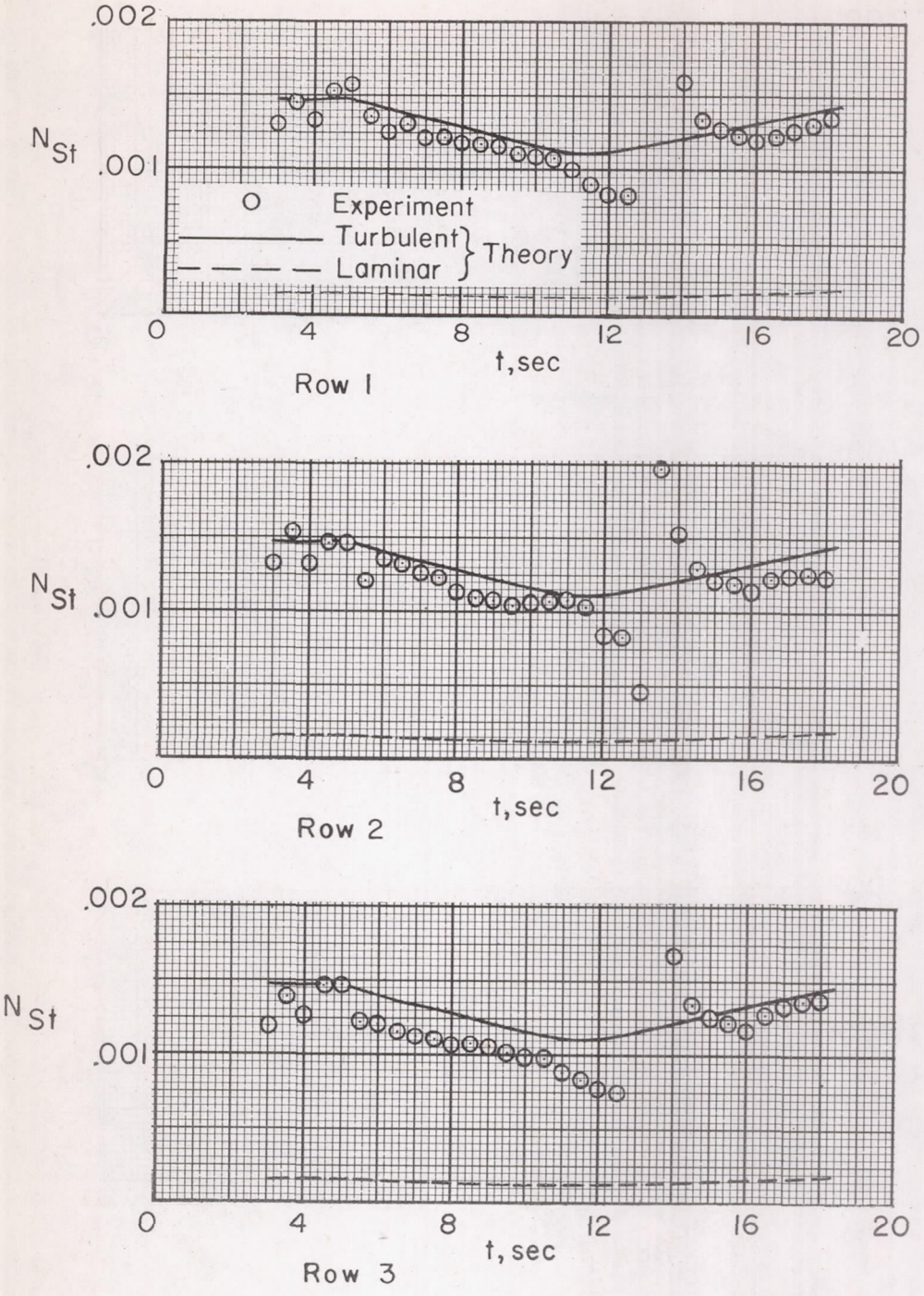






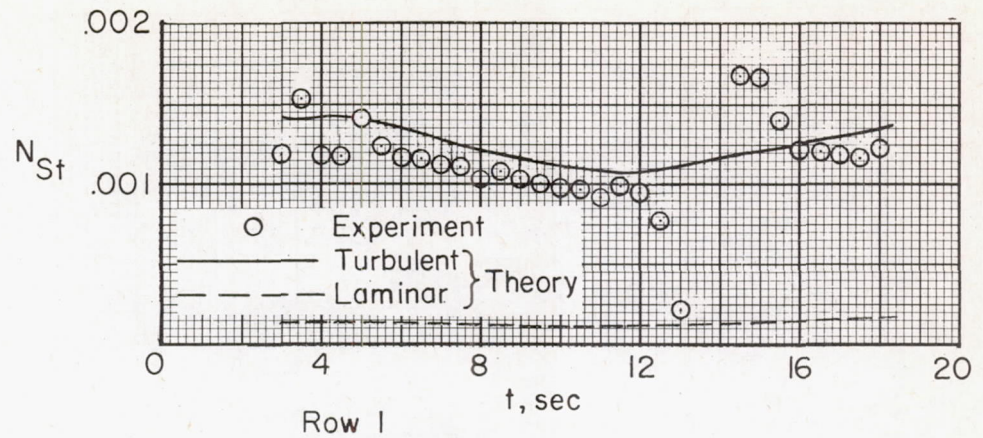
(b) Station 2.

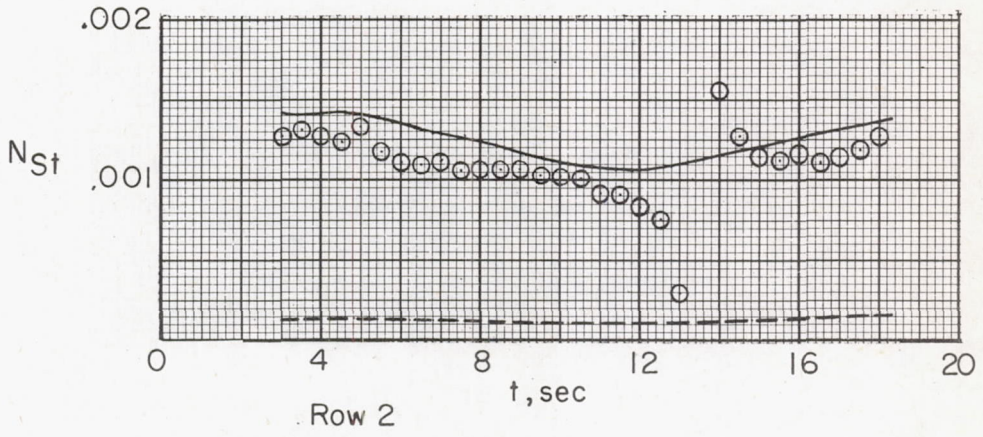
Figure 10.- Continued.

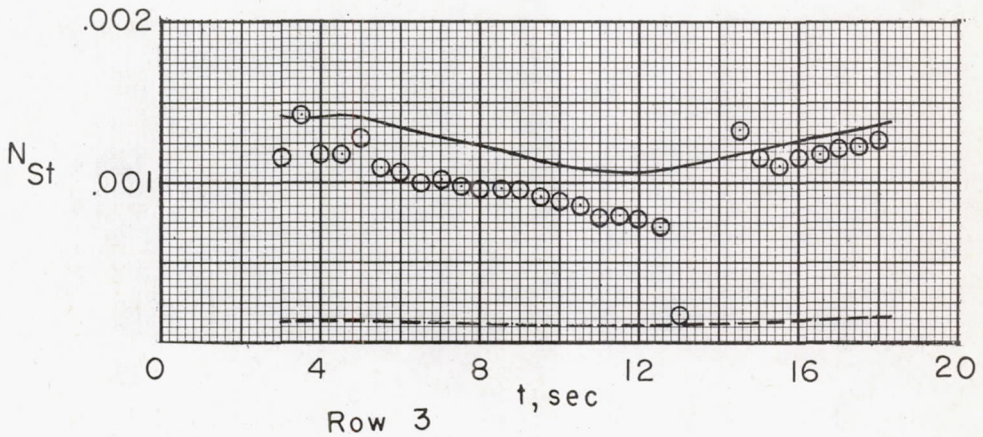


(c) Station 3.

Figure 10.- Continued.

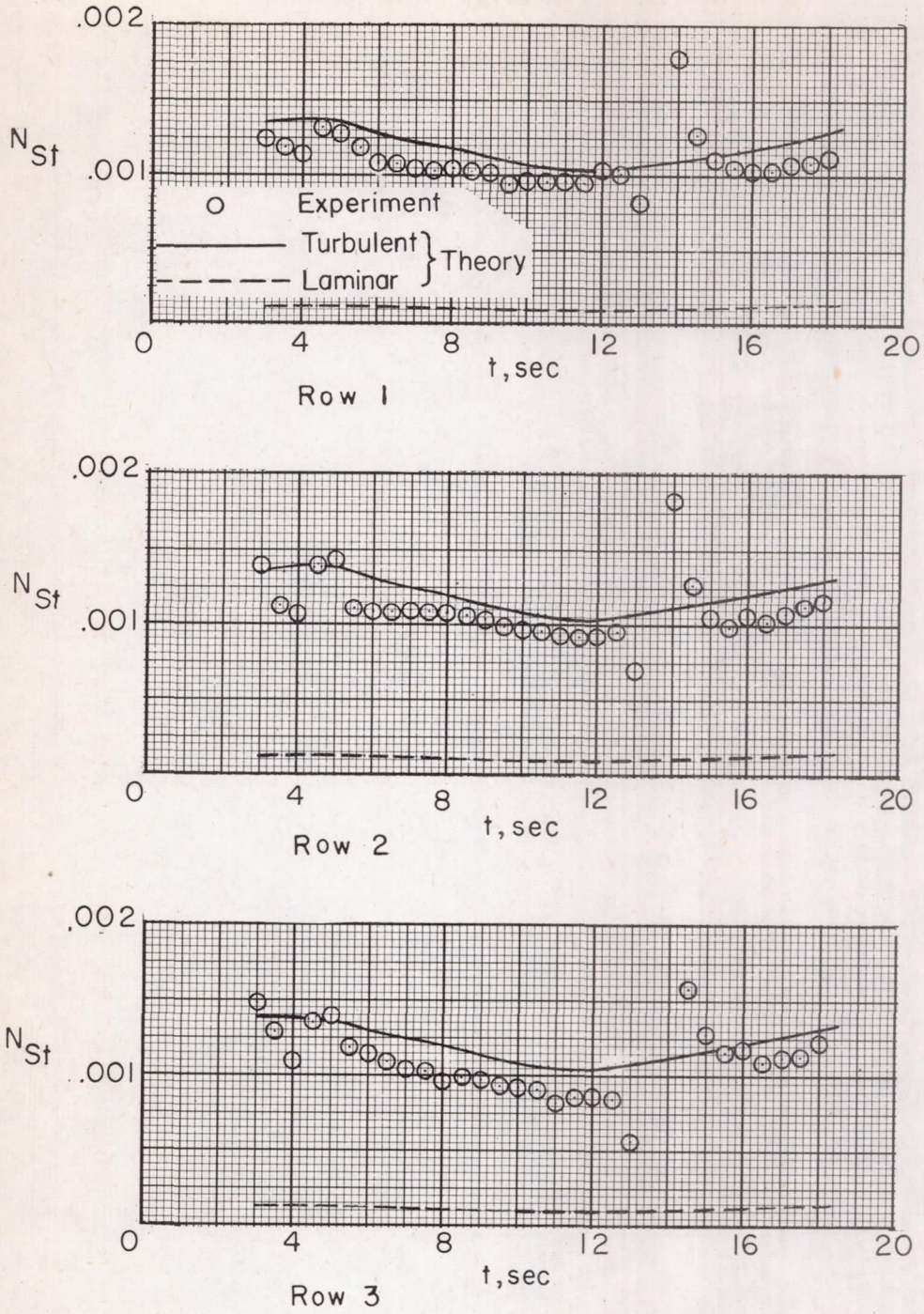






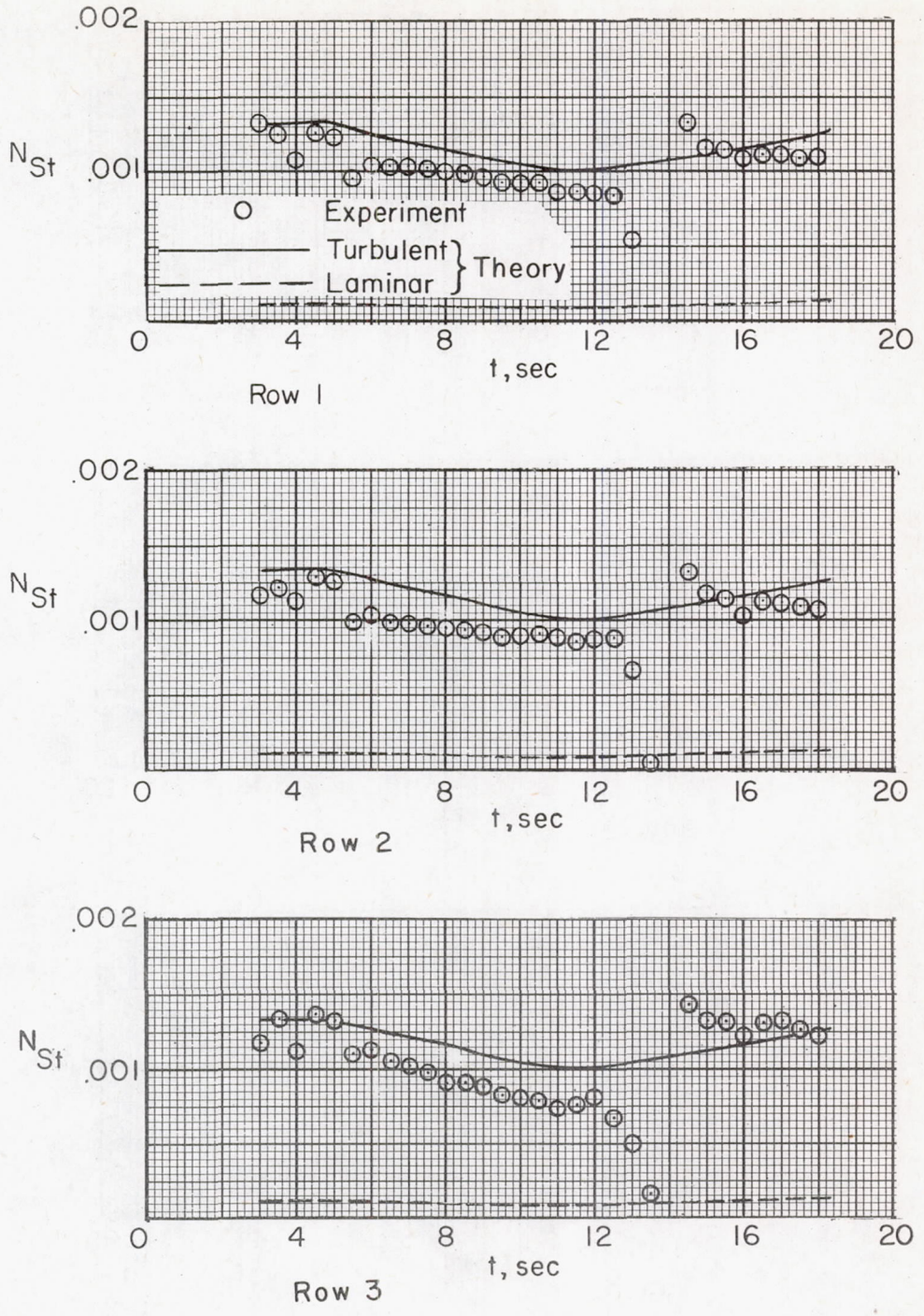
(d) Station 4.

Figure 10.- Continued.



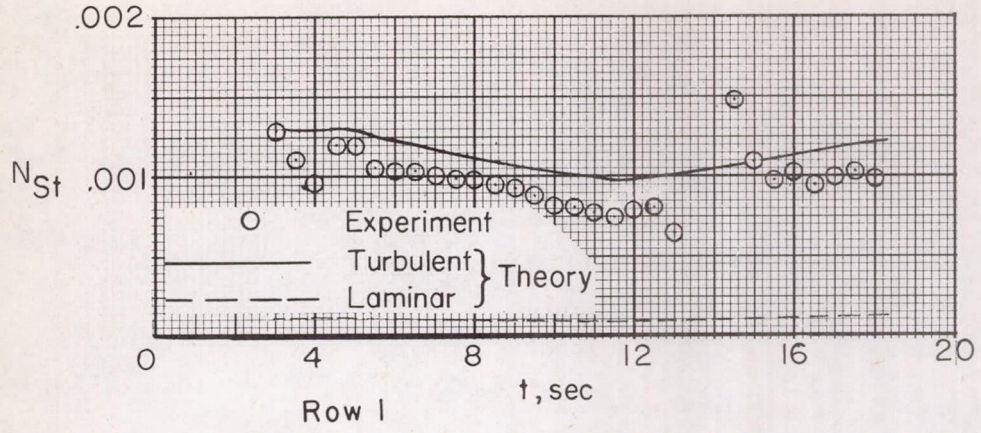
(e) Station 5.

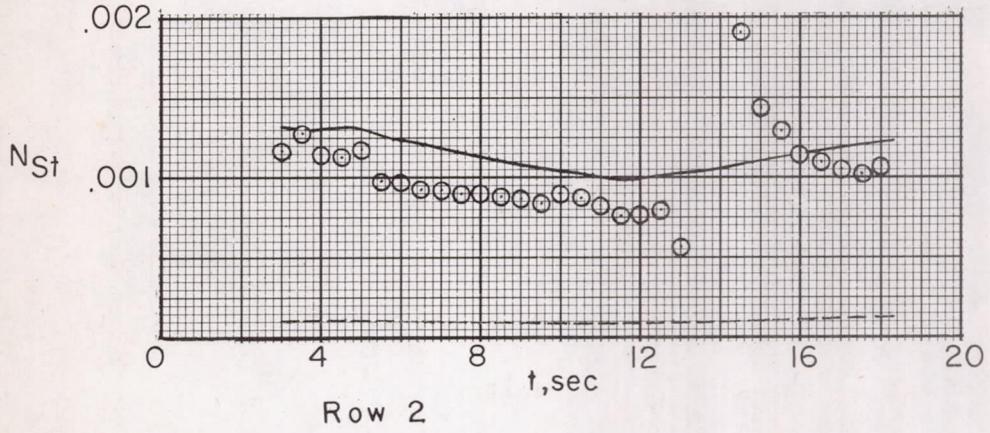
Figure 10.- Continued.

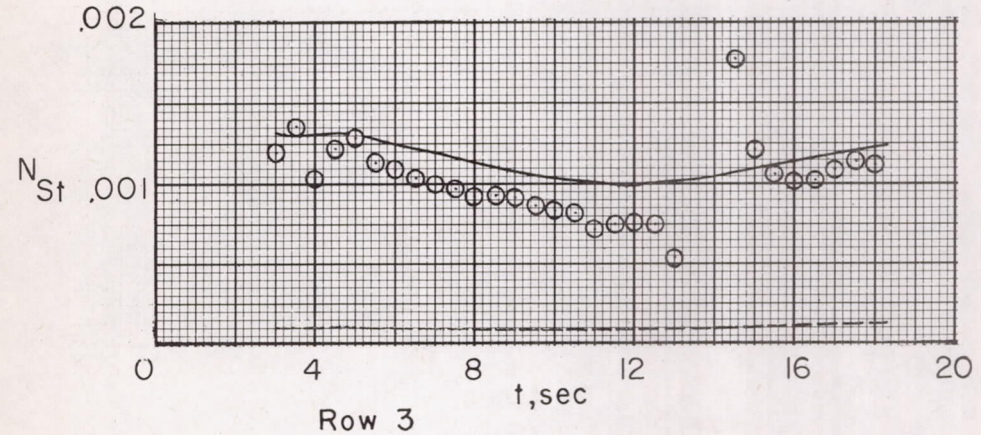


(f) Station 6.

Figure 10.- Continued.

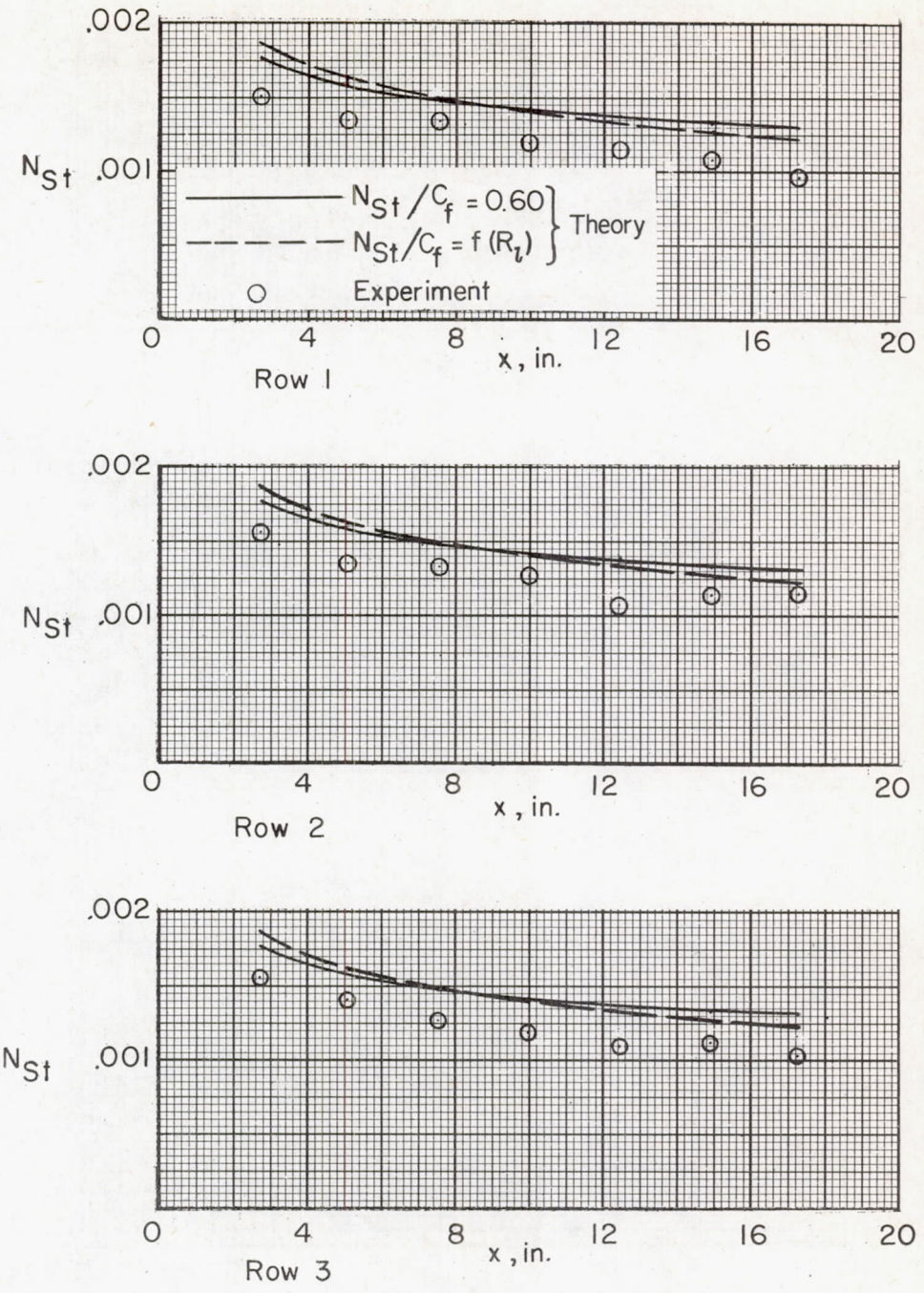






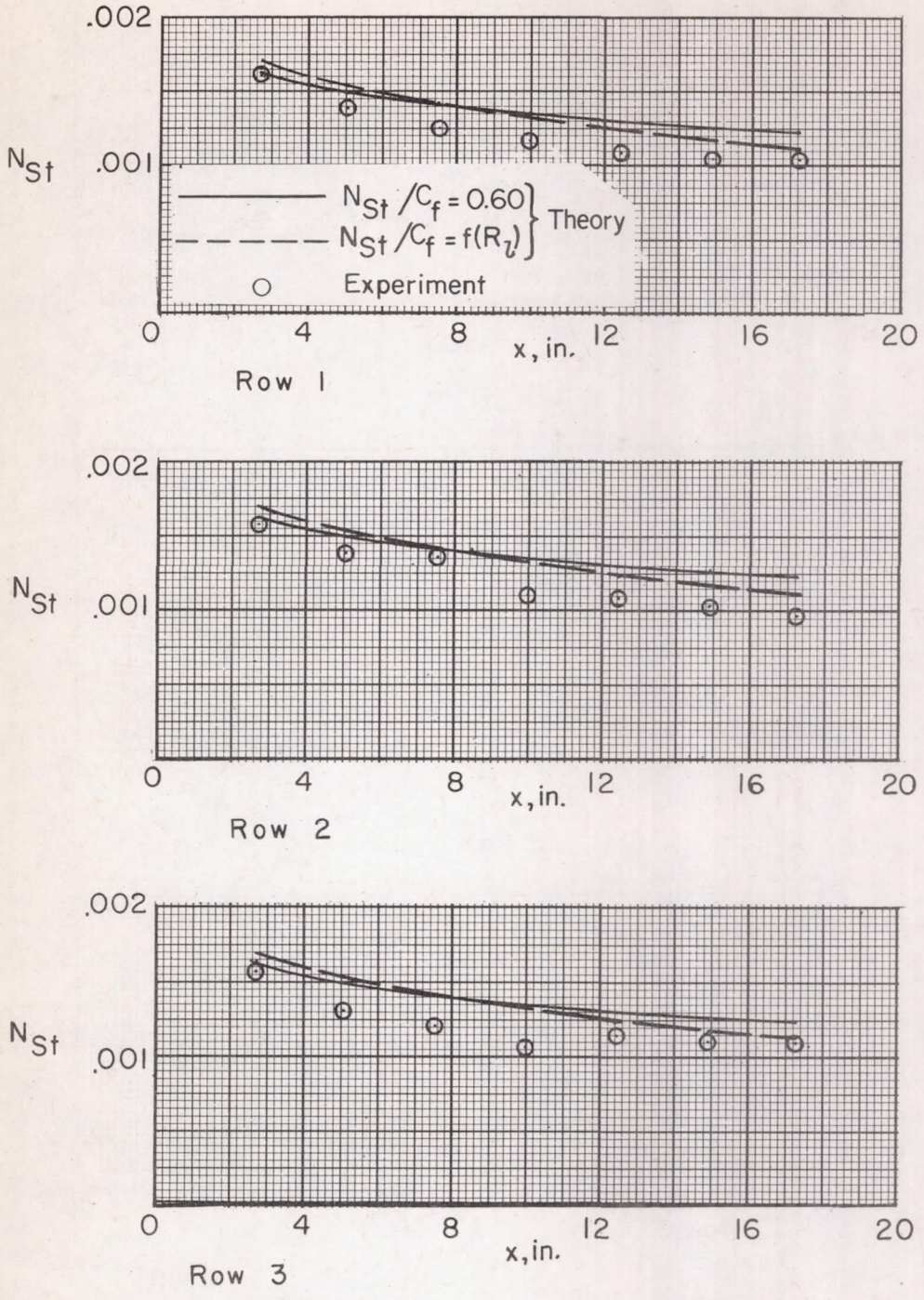
(g) Station 7.

Figure 10.- Concluded.



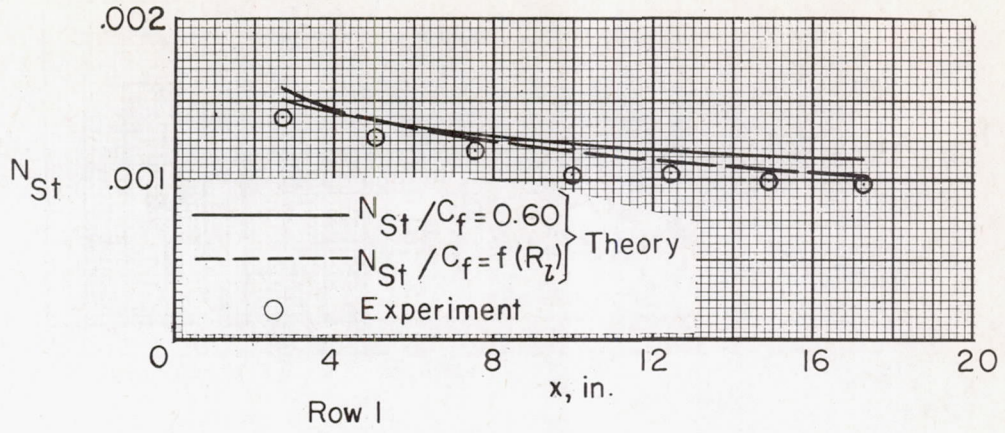
(a) t = 4 seconds; M = 1.52.

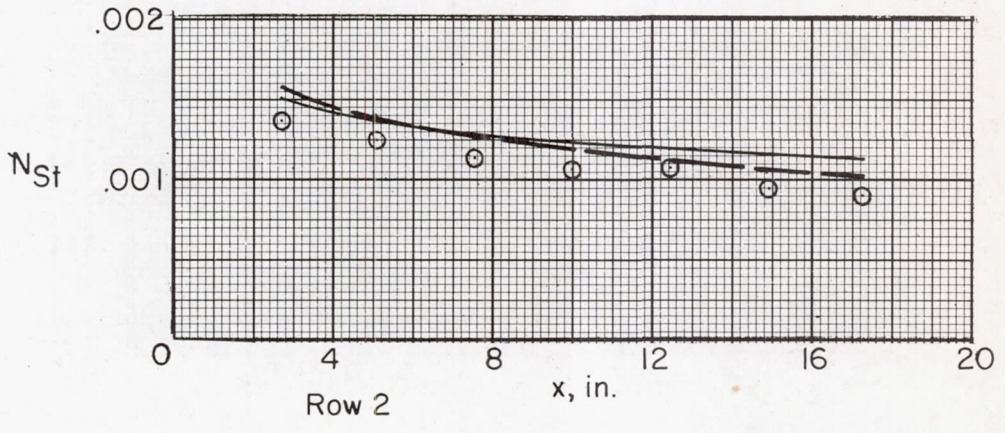
Figure 11.- Variation of Stanton number with distance from wing leading edge for three spanwise locations at various time intervals.

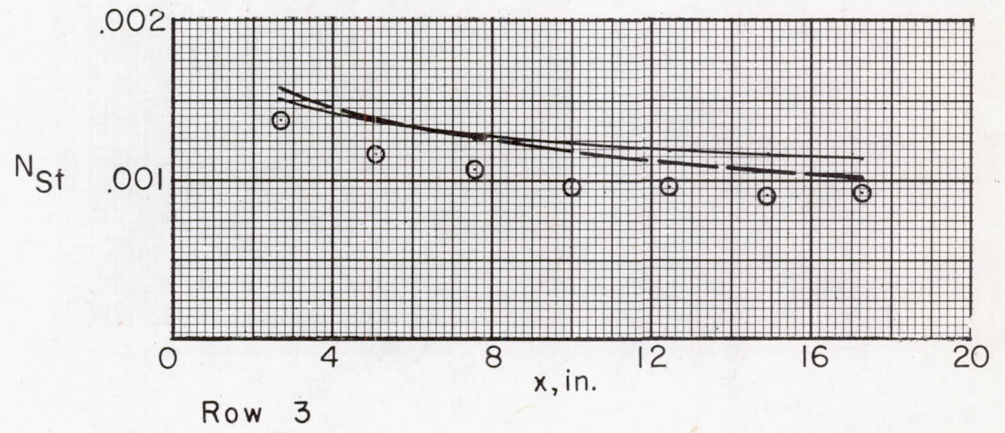


(b) t = 6 seconds; M = 1.76.

Figure 11.- Continued.

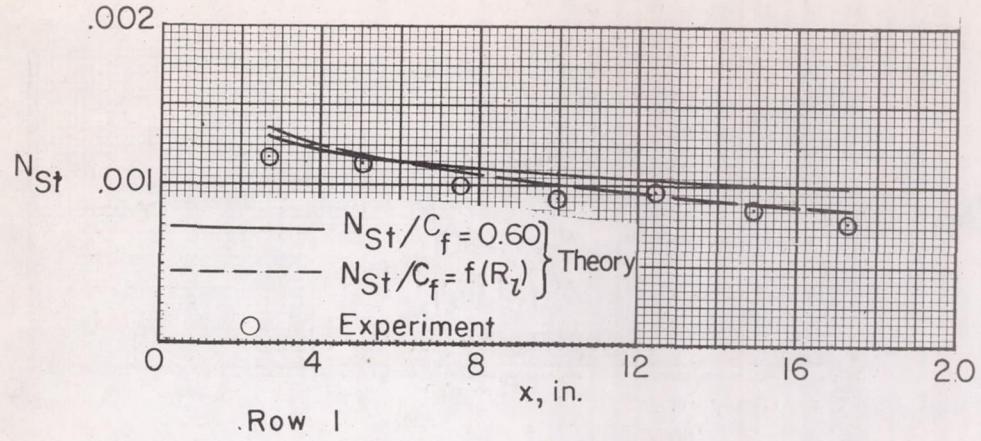


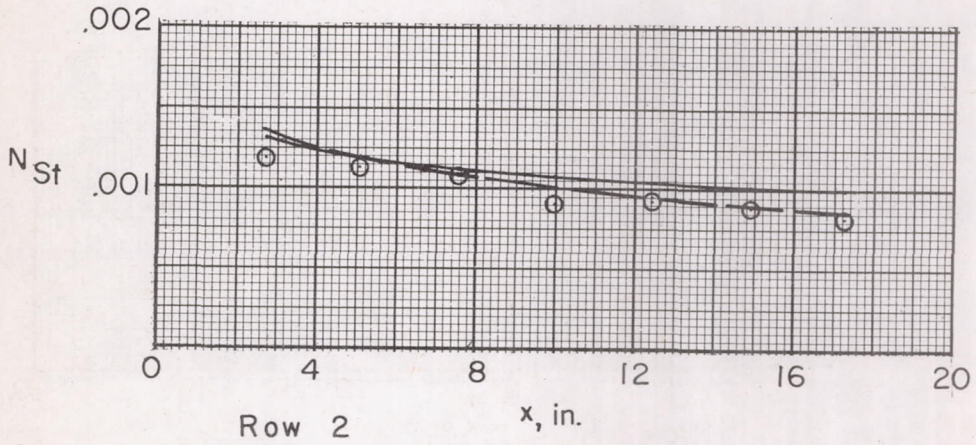


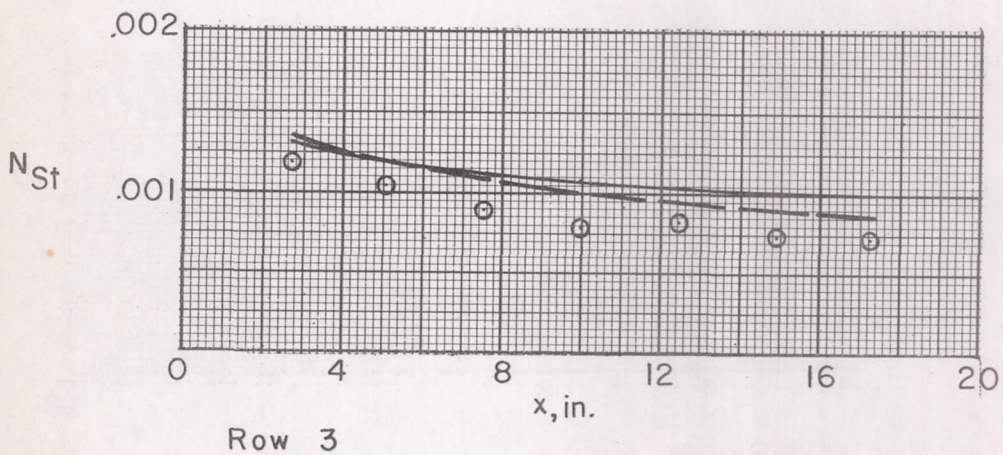


(c) t = 8 seconds; M = 2.13.

Figure 11.- Continued.

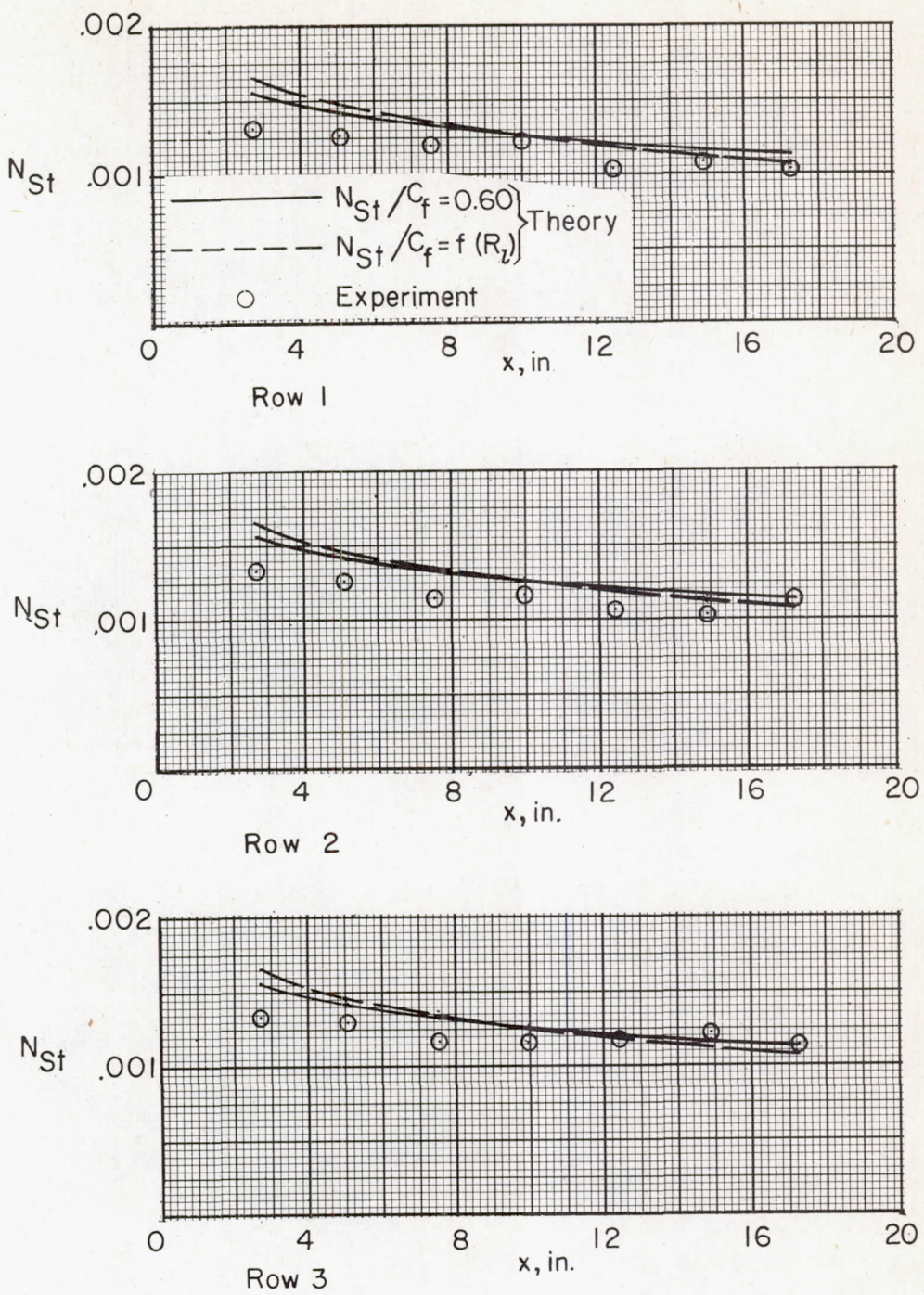






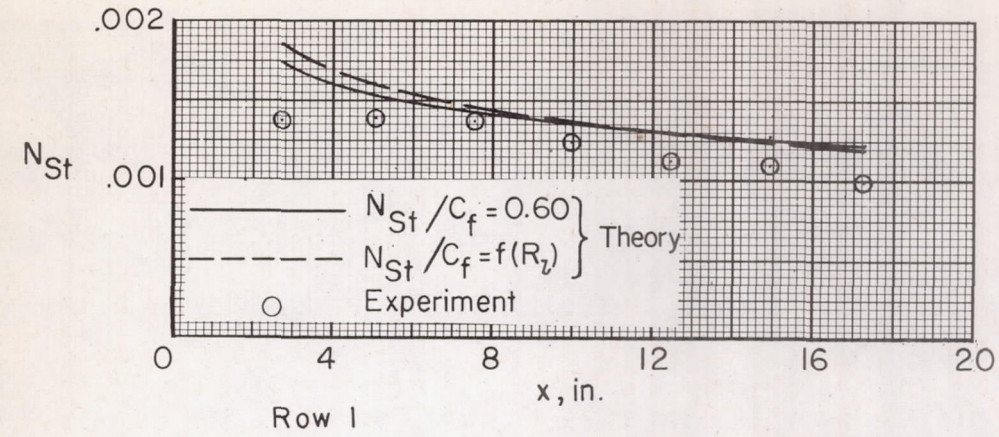
(d) t = 11 seconds; M = 2.66.

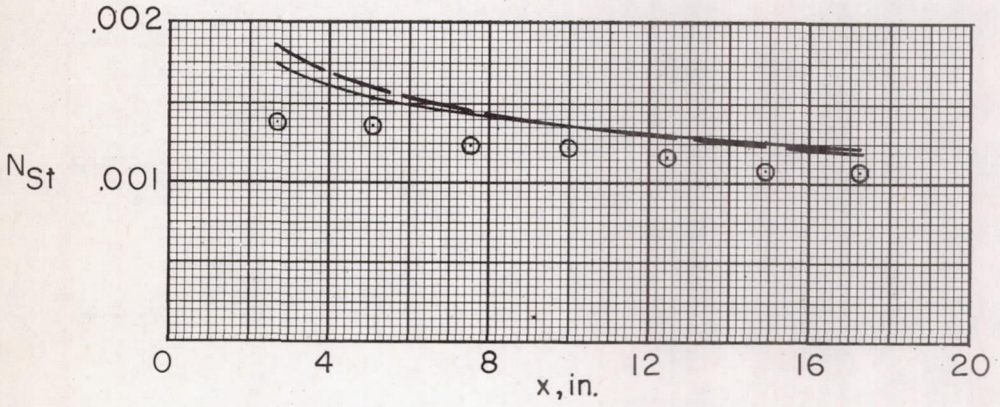
Figure 11.- Continued.

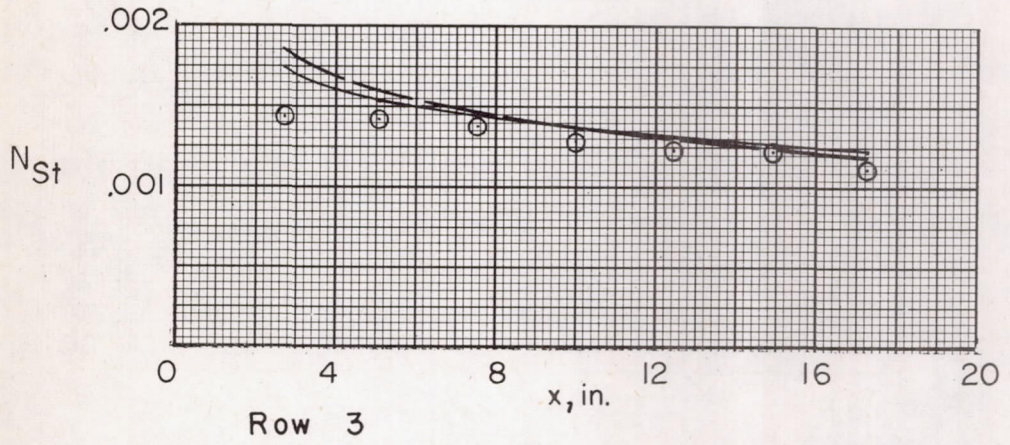


(e) t = 16 seconds; M = 1.54.

Figure 11.- Continued.

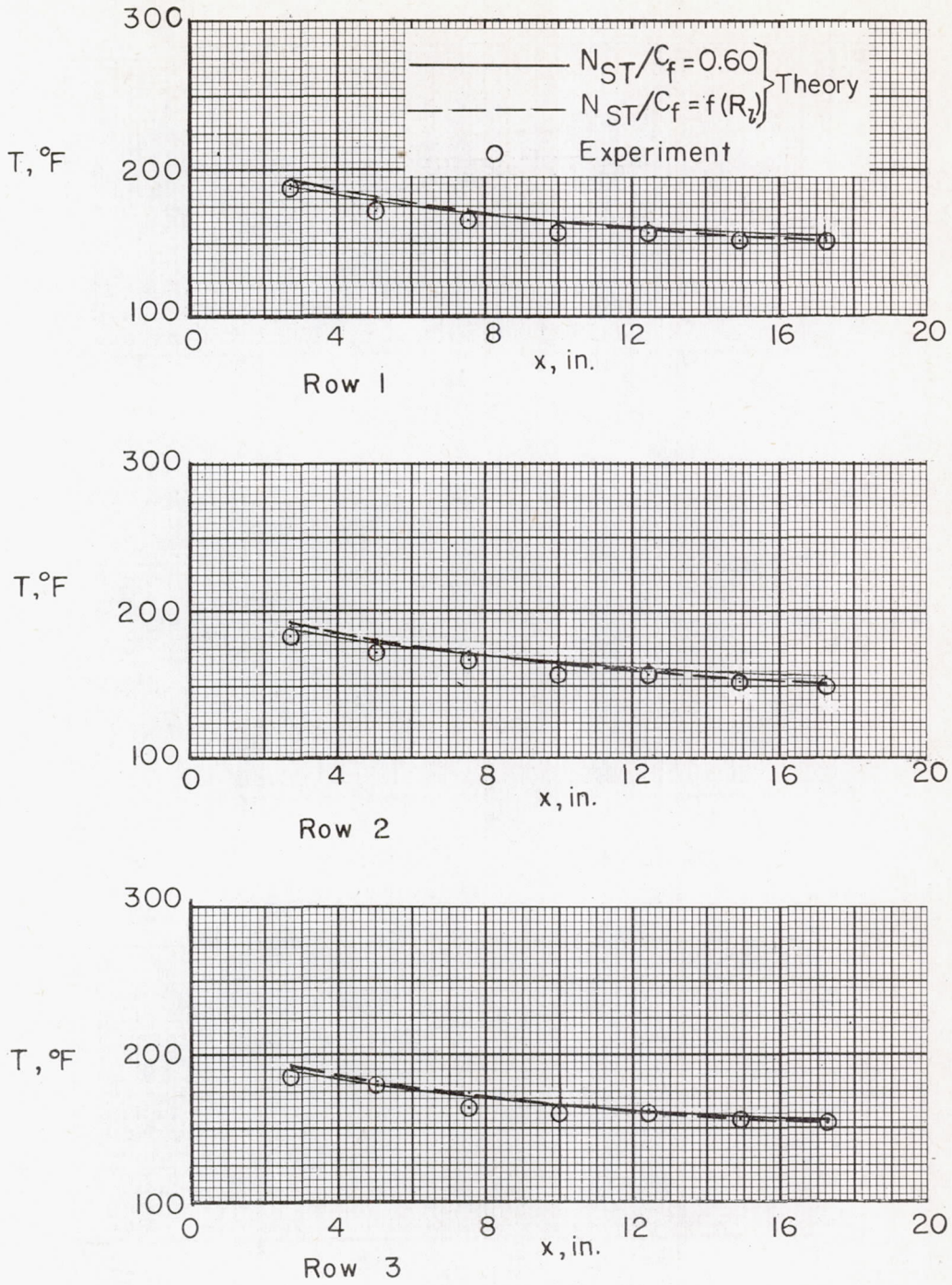






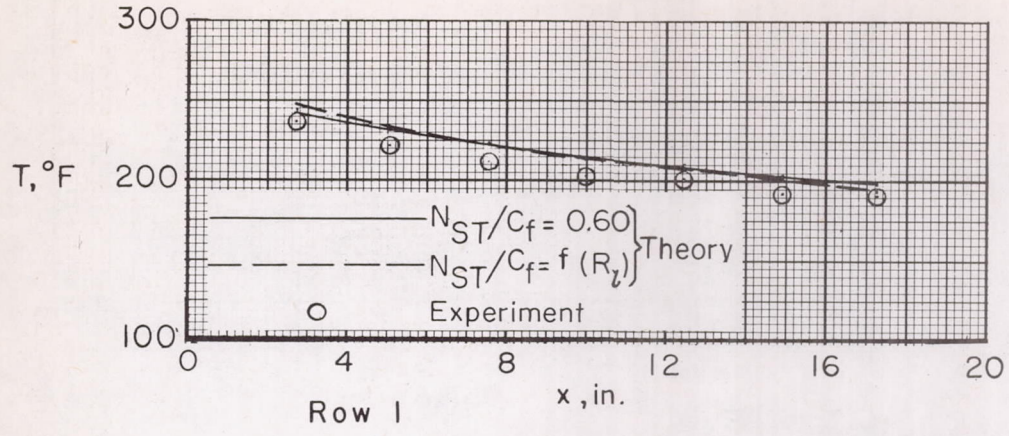
(f) t = 18 seconds; M = 1.23.

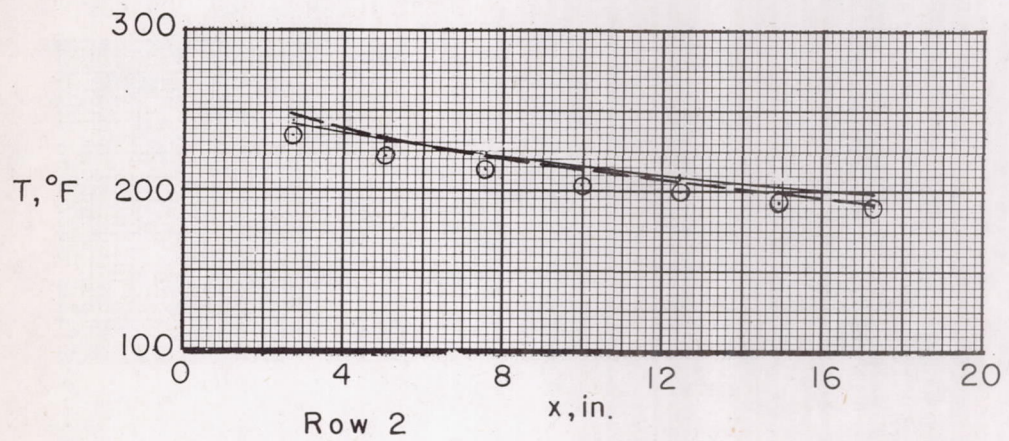
Figure 11.- Concluded.

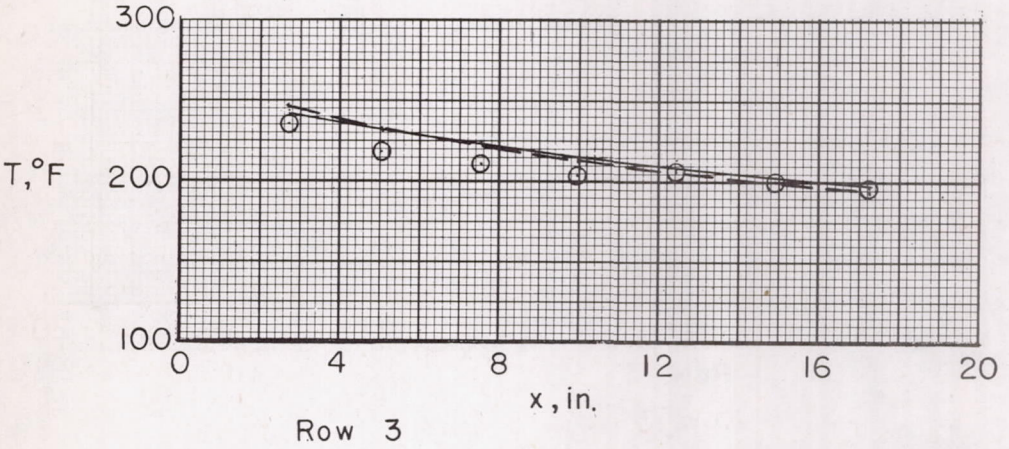


(a) t = 4 seconds; M = 1.52.

Figure 12.- Variation of temperature with distance from wing leading edge at various time intervals. Temperature variation at spars not shown.

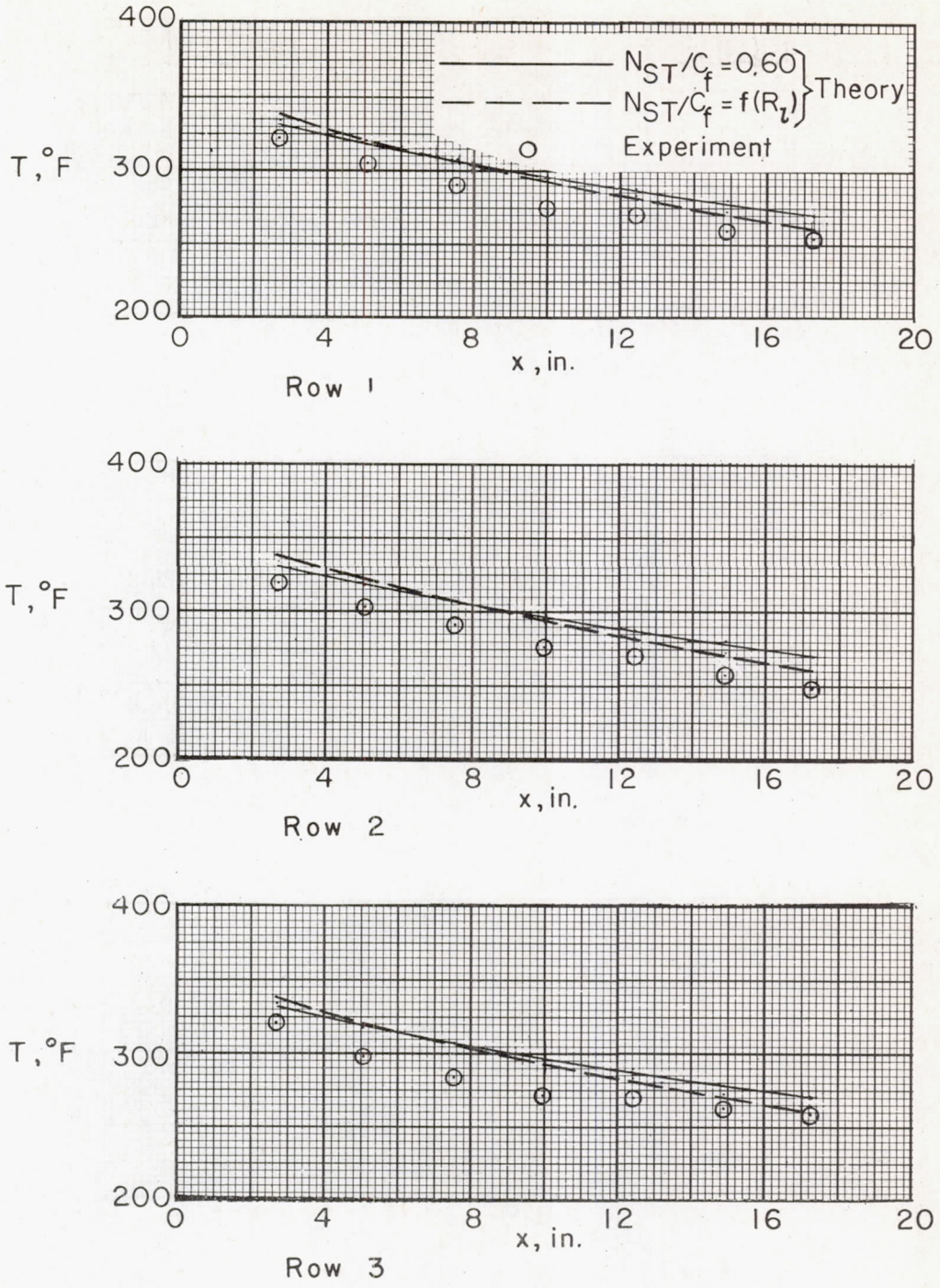






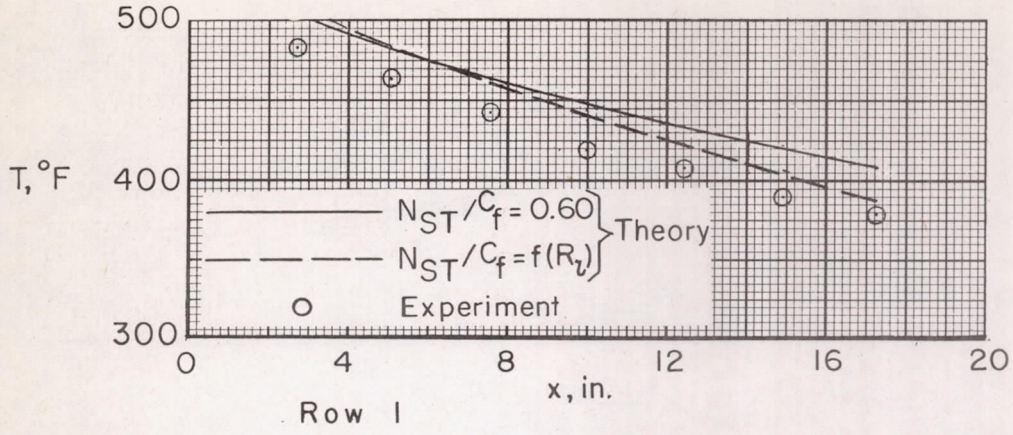
(b) t = 6 seconds; M = 1.76.

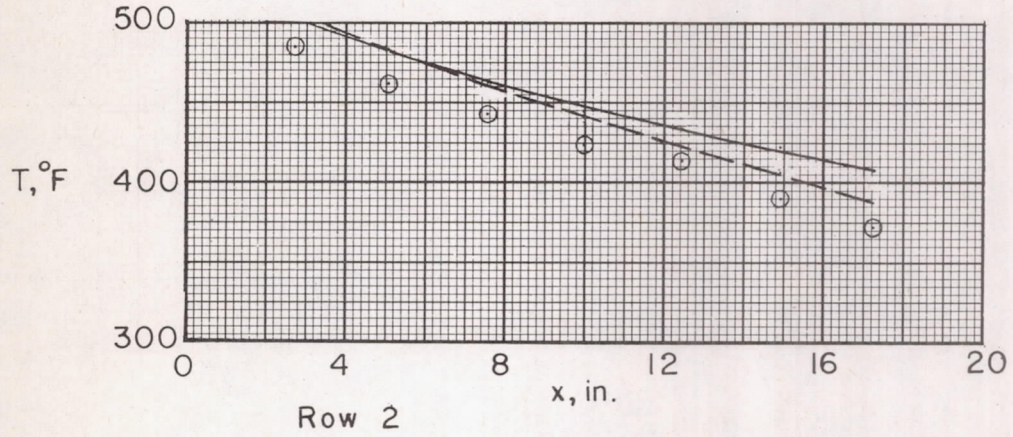
Figure 12.- Continued.

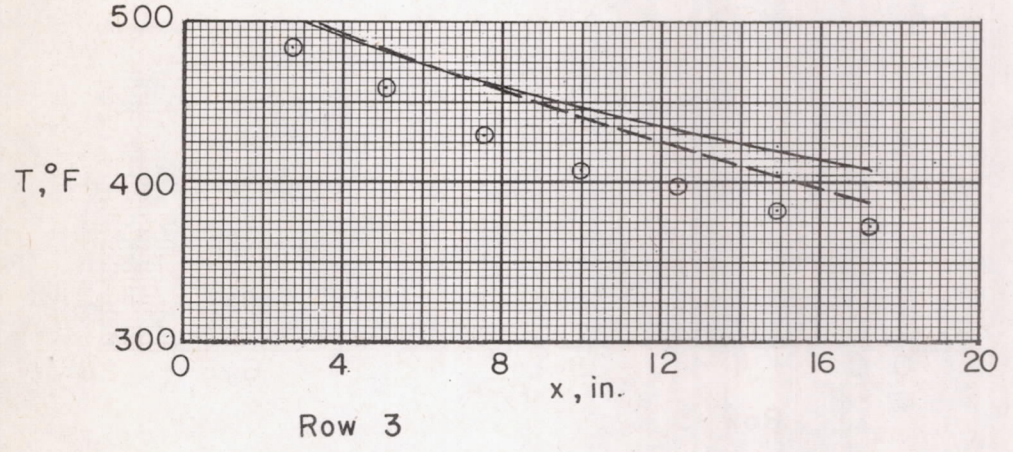


(c) t = 8 seconds; M = 2.13.

Figure 12.- Continued.

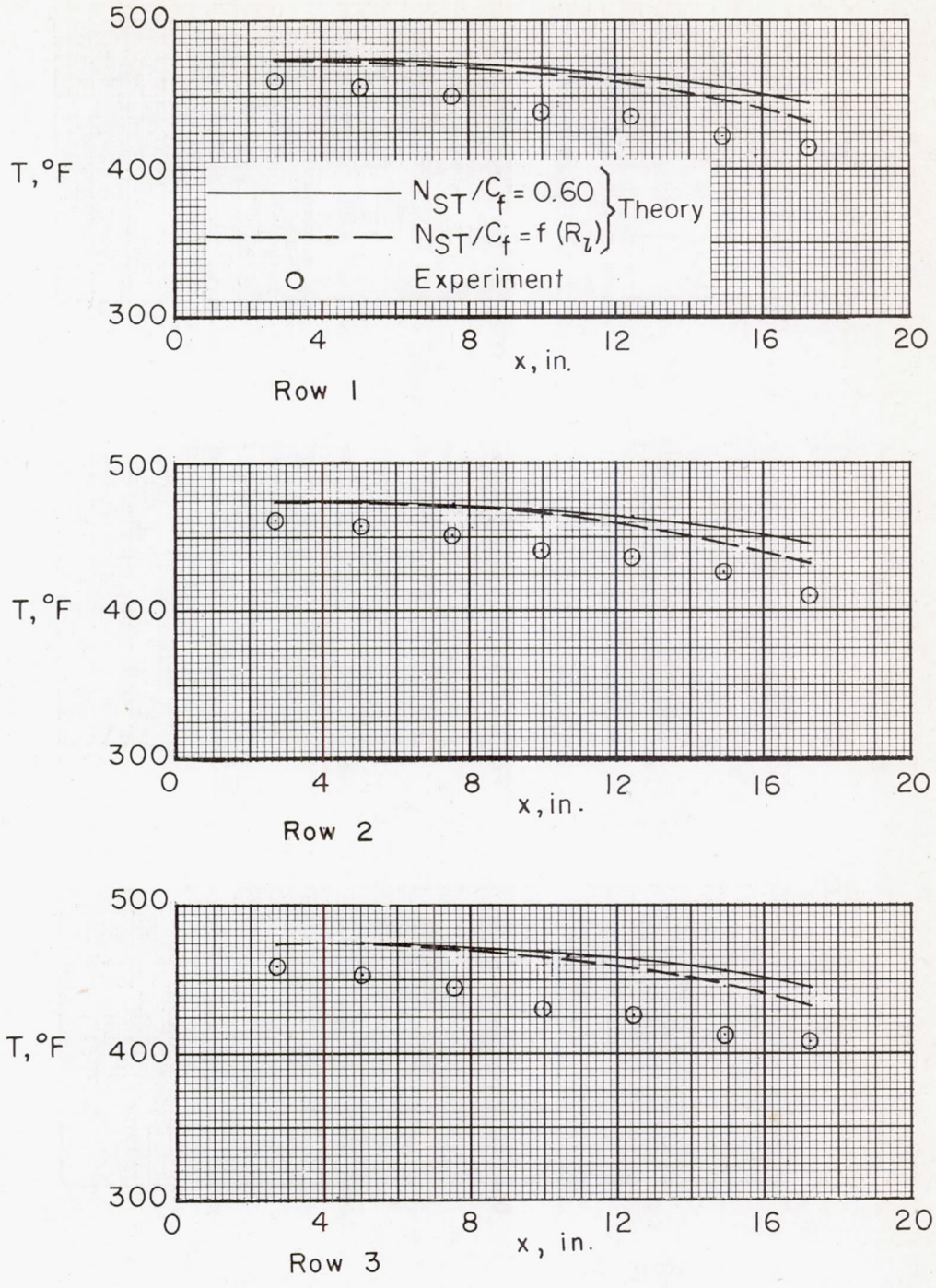






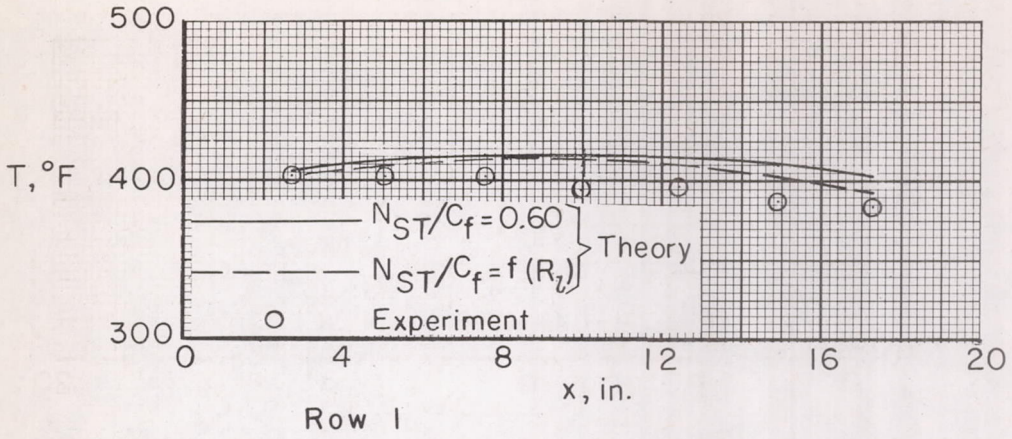
(d) t = 11 seconds; M = 2.66.

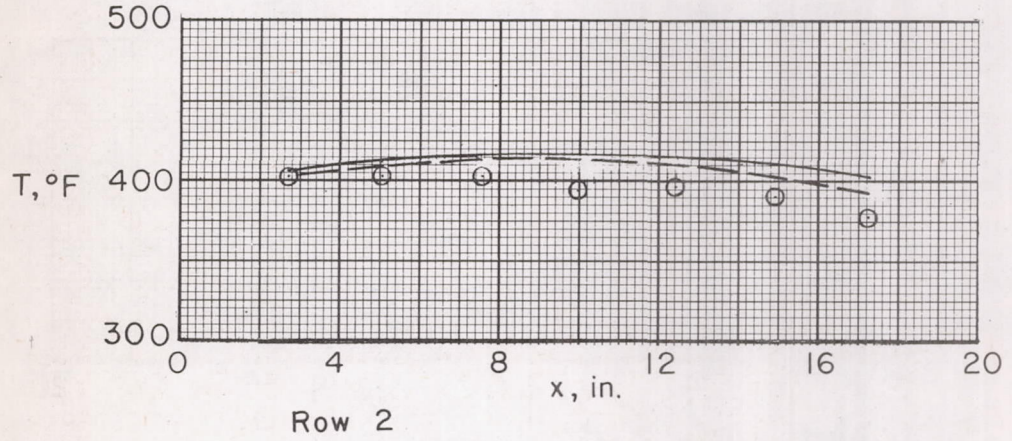
Figure 12.- Continued.

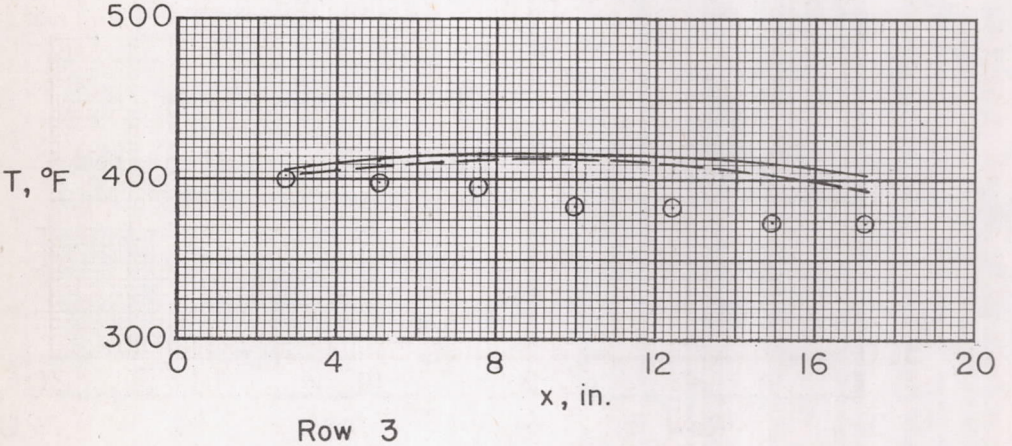


(e) t = 16 seconds; M = 1.54.

Figure 12.- Continued.







(f) t = 18 seconds; M = 1.23.

Figure 12.- Concluded.

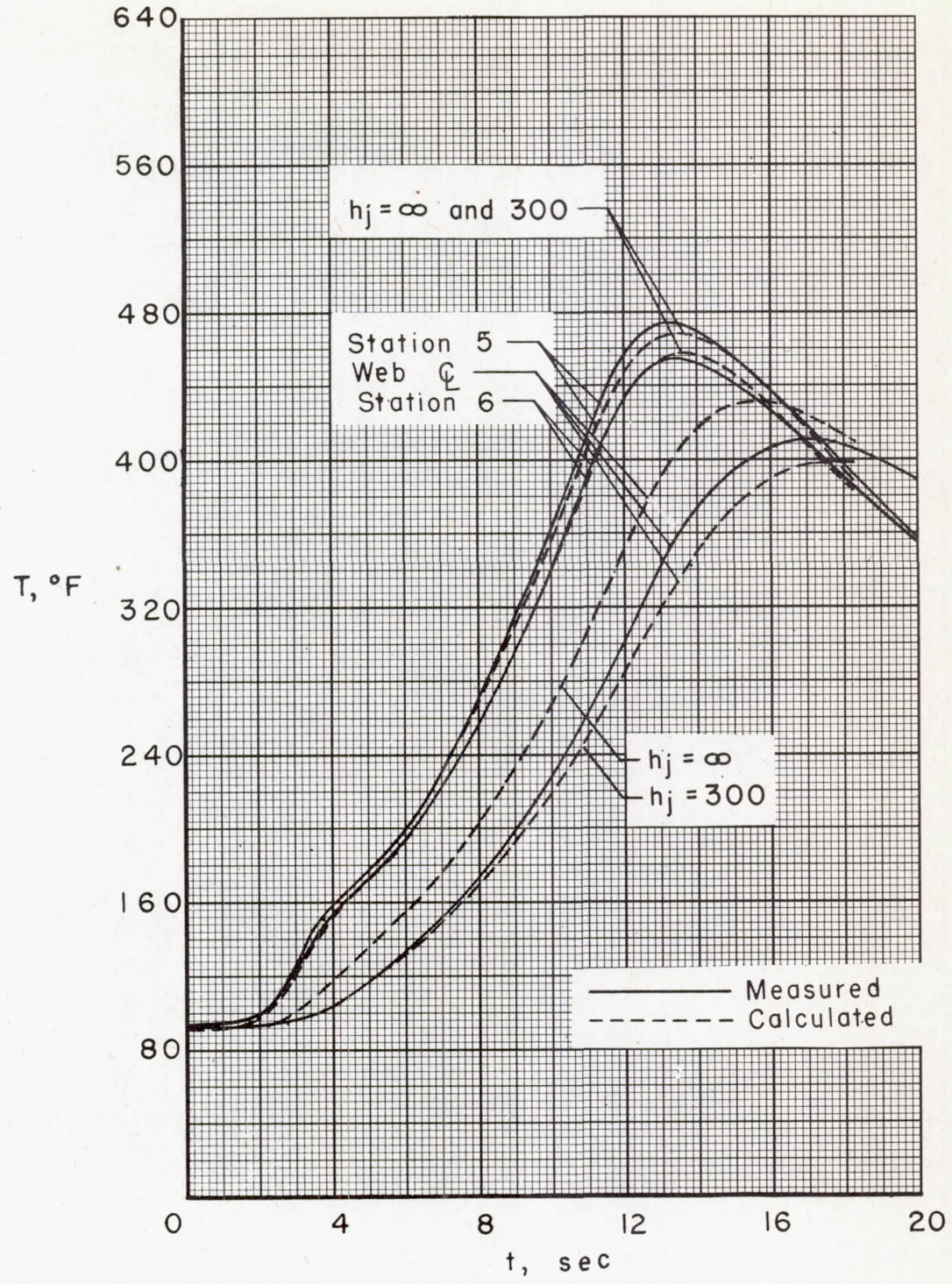


Figure 13.- Comparison of measured temperatures with calculated temperatures for row 2 of stations 5 and 6 and web ℄.

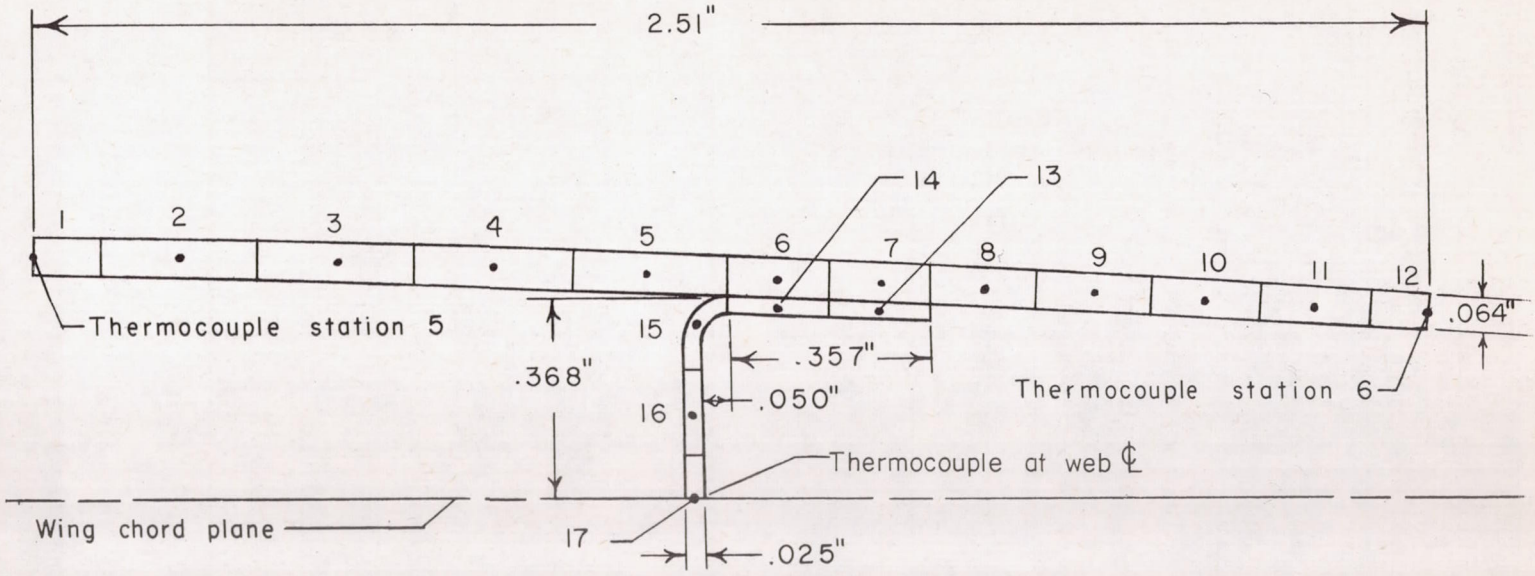
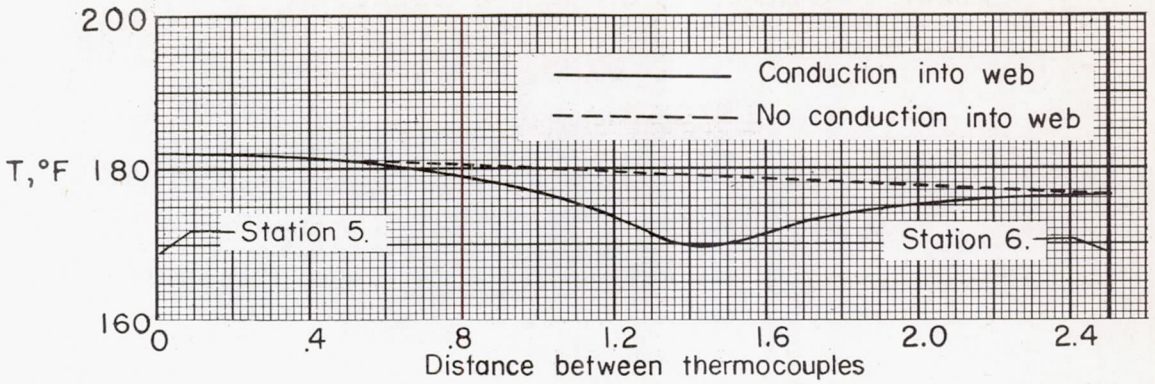
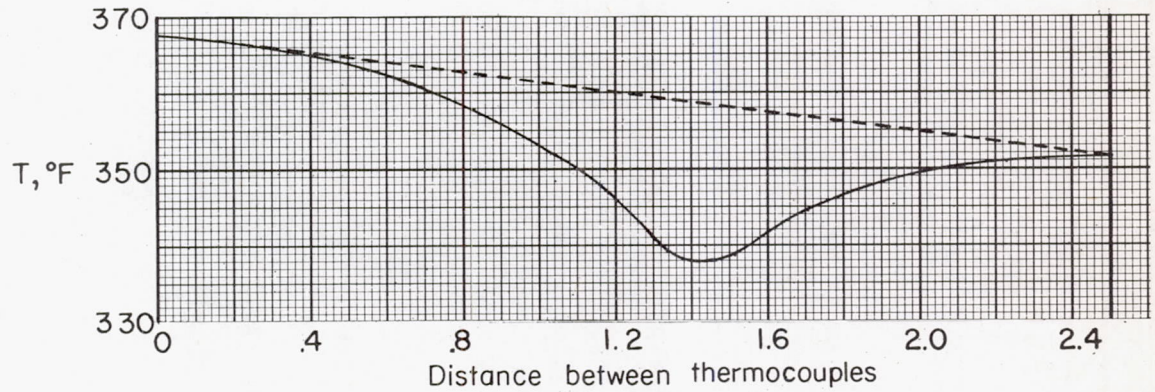


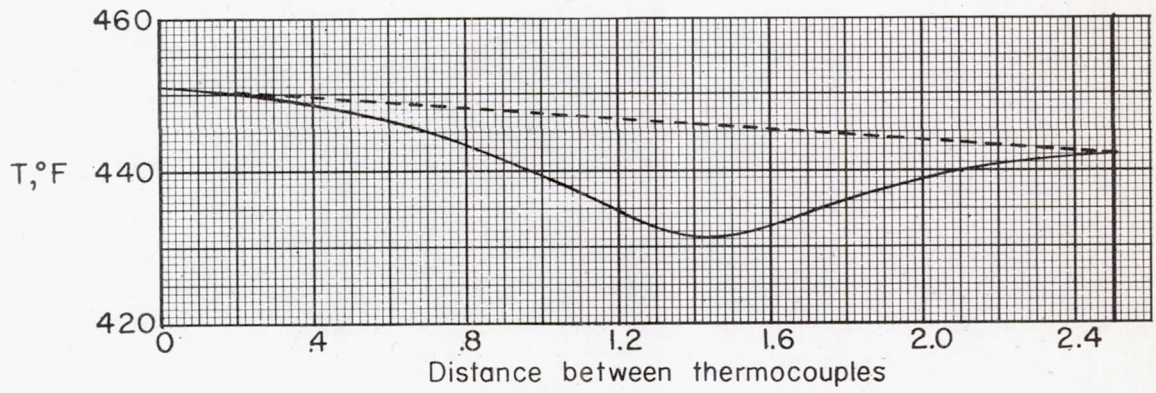
Figure 14.- Section of test wing in vicinity of web thermocouple showing division into elements for calculation purposes.



(a) t = 6.0 seconds; M = 1.76.



(b) t = 11.0 seconds; M = 2.66.



(c) t = 16.0 seconds; M = 1.54.

Figure 15.- Calculated skin temperature variation between stations 5 and 6 showing the effect of heat conduction into spar.

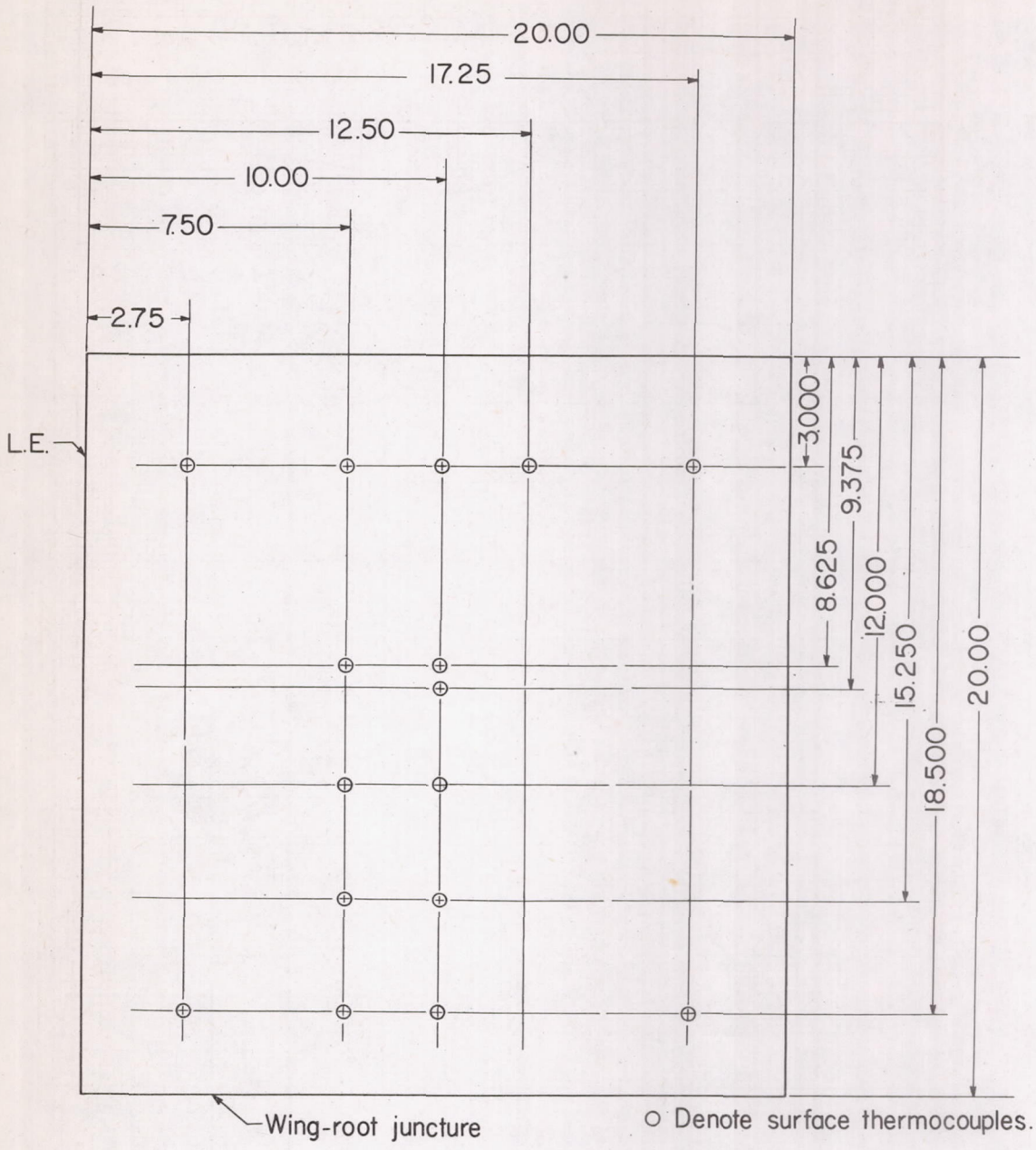


Figure 16.- Instrumentation of test wing for ground test. All dimensions are in inches.

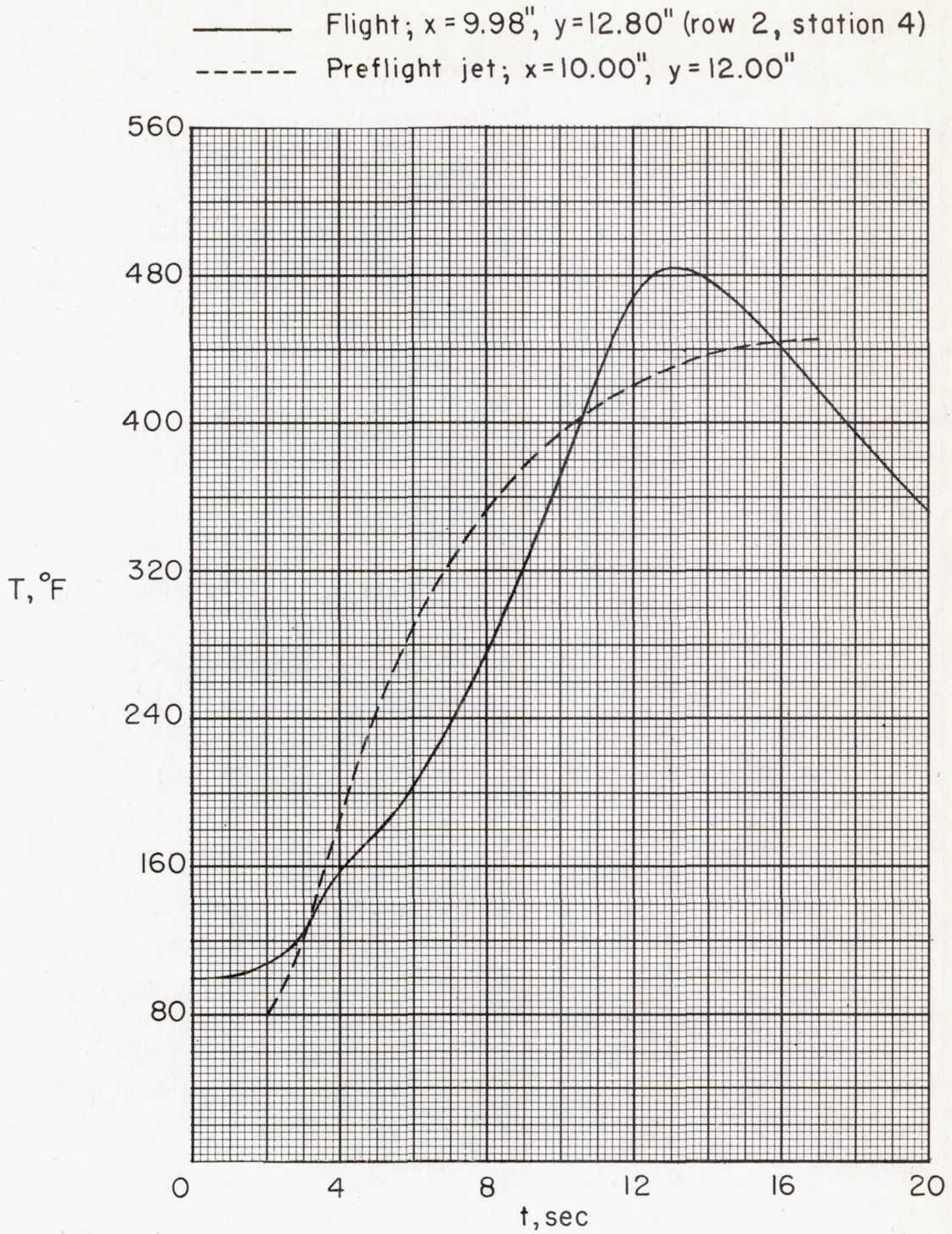


Figure 17.- Illustrative comparison of measured temperatures in flight with values obtained in preflight jet.

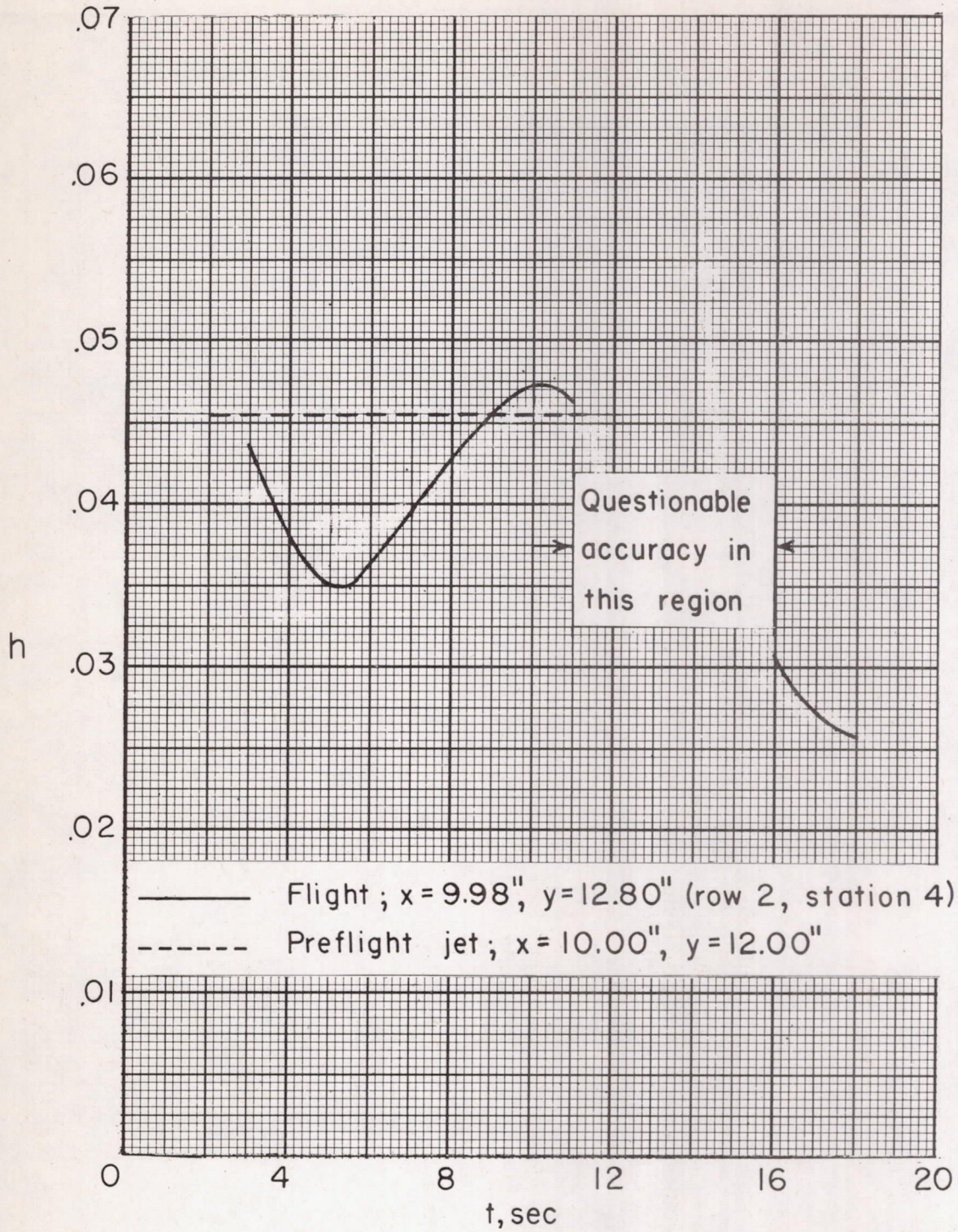


Figure 18.- Comparison of measured heat-transfer coefficients obtained in flight with values obtained in preflight jet.

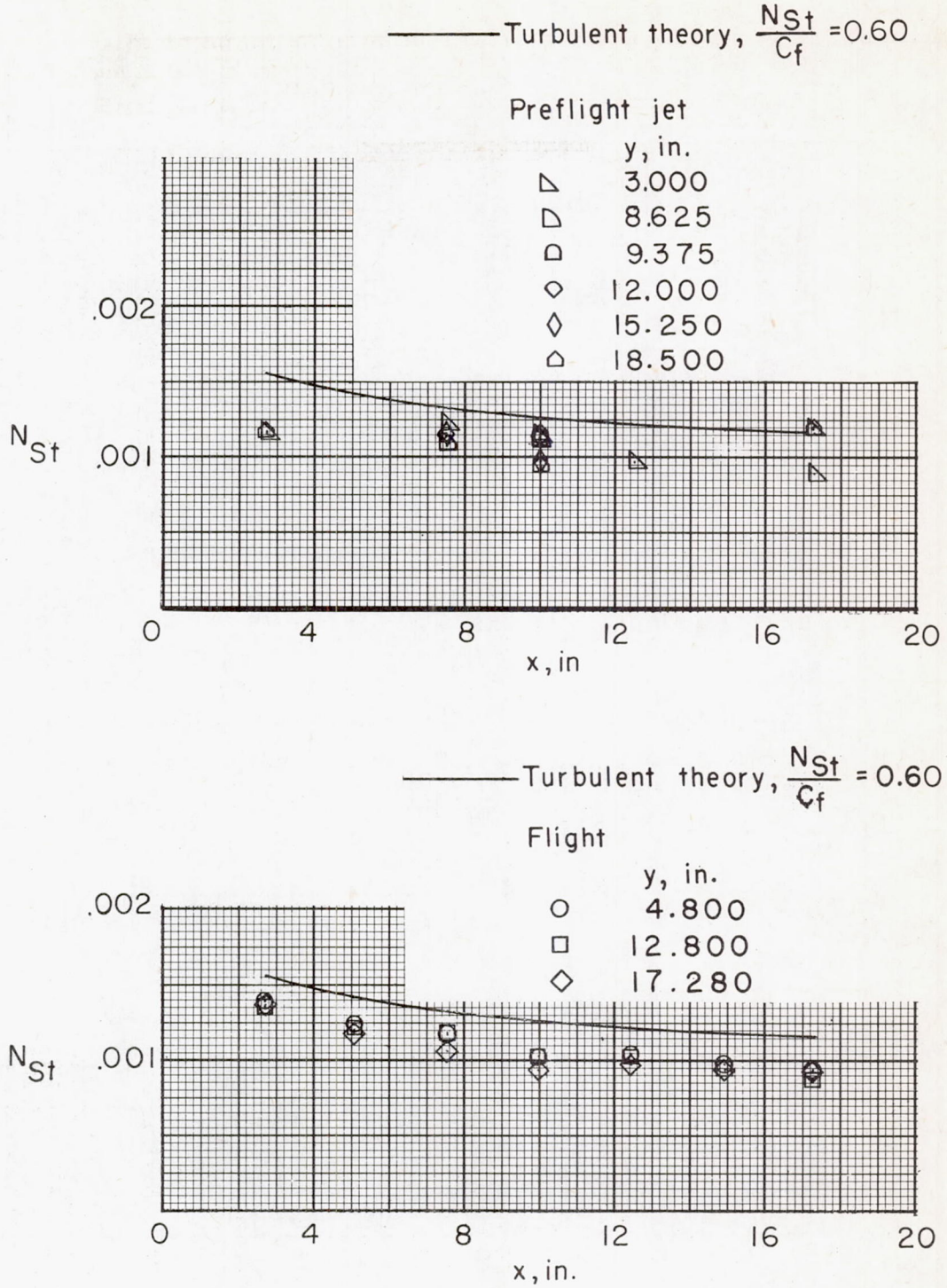


Figure 19.- Comparison of chordwise variation of Stanton number values obtained in flight and preflight jet with turbulent theory. M = 1.99.